



Spectroscopic study of Si-based semiconductor  
heterostructures grown by molecular beam epitaxy

(分子線エビタキシー法により作製した Si 系ヘテロ構造の分光学的研究)

NUMATA, USAMI

①  
学位請求論文

Spectroscopic study of Si-based semiconductor  
heterostructures grown by molecular beam epitaxy

(分子線エピタキシー法により作製したSi系ヘテロ構造の分光学的研究)

A Dissertation for  
the degree of Doctor of Engineering

by

Noritaka USAMI

宇佐美 徳隆

12 November, 1997

## Acknowledgments

First of all, the author would like to express his hearty appreciation to Prof. Y. Shiraki for his sincere guidance throughout the work.

The author is grateful to Profs. R. Ito, K. Onabe, and T. Osada for their guidance and helpful discussions.

The author expresses his sincere gratitude to Profs. E. Hanamura, N. Miura, and K. Nakagawa for helpful discussions on this thesis.

The author is very happy to express his hearty thanks to Prof. S. Fukatsu for his collaboration throughout this work, helpful instructions on the experiments, and fruitful discussions.

Profs. H. Akiyama and H. Sakaki are gratefully acknowledged for their cooperation in time-resolved photoluminescence spectroscopy and fruitful discussions.

T. Mine is acknowledged for his collaboration in fabrication of quantum wires and fruitful discussions.

Dr. V. Higgs is acknowledged for his collaboration in cathodoluminescence measurements and fruitful discussions.

Dr. D. K. Nayak is acknowledged for his collaboration in strained-Si/relaxed-SiGe quantum wells, and his guidance in English conversation.

Dr. H. Yaguchi is gratefully acknowledged for his instructions on the experiments and fruitful discussions.

Dr. K. Fujita is gratefully acknowledged for his instructions on the experiments, especially on the operation of MBE, and many stimulating discussions.

S. Ohtake is gratefully acknowledged for his technical support especially on the maintenance of the clean room.

Dr. H. Sunamura is gratefully acknowledged for fruitful discussions and good partnership for the operation of our gas-source MBE system.

E. S. Kim is gratefully acknowledged for his helpful discussions, friendship, and technical support throughout the work.

Drs. K. Muraki, A. Fujiwara, B.P. Zhang, S. Miyoshi are gratefully acknowledged for their guidance through their stimulating researches.

Prof. F. Minami, and H. Ito are acknowledged for their instructions on time-resolved photoluminescence spectroscopy, photoluminescence under high pressure, and fruitful discussions.

Y. Shimooka, Dr. W. Pan, and M. Nagahara are acknowledged for their guidance on the photolithography processing and their friendship.

"Kaz." Ota and "Teru." Ota are gratefully acknowledged for fruitful discussions.

Technical support of A. Yutani, G. Ohta, Y. Ebuchi, J. Arai, T. Ueno, K. Amano, M. Miura, A. Ohga is gratefully acknowledged.

The author is indebted to Dr. J. Y. Kim, Dr. Z. Ji, K. Shiraishi, T. Osabe, H. Yoshida, F. Isshiki, T. Sugita, T. Kimura, and to all the members of the photonic materials, and to the staff of the administrative office of RCAST for the completion of this thesis.

Finally, the author expresses his hearty thanks to his wife, Michiyo, and for his mother, Michiko, for their continuous encouragement.

## Table of Contents

<i>Acknowledgments</i>	<i>i</i>
<b>1. Introduction</b>	<b>1</b>
1.1 Motivation: Why SiGe?	1
1.2 Organization	2
<b>2. Strained-Si<sub>1-x</sub>Ge<sub>x</sub>/Si heterostructures : An overview</b>	<b>5</b>
2.1 Band modification by SiGe/Si heterostructures	5
2.1.1 Strains	5
2.1.2 Valence band	6
2.1.3 Conduction band	8
2.1.4 Bandgap	9
2.1.5 Band alignment	10
2.2 Epitaxial growth of SiGe/Si by Molecular Beam Epitaxy	13
2.2.1 Solid-source MBE	13
2.2.2 Gas-source MBE	13
2.2.3 Ge surface segregation	15
2.2.4 Segregant Assisted Growth	16
2.3 Photoluminescence of strained-Si <sub>1-x</sub> Ge <sub>x</sub> /Si quantum wells	19
<b>3. Neighboring Confinement Structure</b>	<b>21</b>
3.1 Introduction	21
3.2 Experiment	24
3.3 Photoluminescence: General feature	27
3.4 The origin of the NP enhancement in NCS	32
3.5 NCS with pure-Ge/pure-Si active layer	43
3.6 Summary	47

<b>4. SiGe/Si Quantum Wires on V-groove patterned substrates</b>	<b>48</b>
4.1 Introduction	48
4.2 Fabrication of quantum wires	49
4.3 Photoluminescence and Cathodoluminescence	53
4.4 Exciton diffusion	57
4.5 Selective epitaxial growth of quantum wires	63
4.6 Summary	65
<b>5 Strain-induced quantum nanostructure</b>	<b>66</b>
5.1 Introduction	66
5.2 Lateral band gap modulation by Ge island stressor	67
5.3 Control of Ge island formation by cleaved edge overgrowth	70
5.4 Summary	75
<b>6. Conclusions</b>	<b>76</b>
<i>References</i>	78
<i>List of awards, publications, and presentations</i>	83

## 1. Introduction

### 1.1 Motivation: Why SiGe?

The main goal of research on silicon photonics is to merge Si-based optical devices with advanced commercial Si technology and to integrate optics and electronics on the same Si substrate [1]. The resultant chip would show new functionality compared to the optical and electrical circuits alone. A promising candidate to realize this superchip is to utilize SiGe/Si heterostructures [2] since the careful design and the precise control of the structures with atomic scale can create new physical properties. This "band-engineering" concept is now widely studied on various kinds of heterostructures (III-V, IV-IV, II-VI) owing to the recent progress of growth techniques, such as molecular beam epitaxy (MBE), metalorganic chemical vapor deposition, and ultrahigh vacuum chemical vapor deposition (UHVCVD). It was first considered that to grow SiGe alloys on Si substrates is difficult due to the large lattice mismatch ( $\approx 4.2\%$ ) between Si and Ge, however, strained-SiGe layers can now be grown on Si substrates by various growth techniques without introducing misfit dislocations up to the critical thickness. The large lattice mismatch is not an obstacle but can be regarded as an advantage of the  $\text{Si}_{1-x}\text{Ge}_x/\text{Si}$  heterostructures since the strain gives additional flexibility to the band-engineering. The strained-layer growth of SiGe layers on Si (100) substrates drastically reduces the fundamental indirect band gap than that of the unstrained SiGe alloys. This means that the bandgap can be tuned to the  $1.30\mu\text{m}$  to  $1.55\mu\text{m}$  fiber-optic communications range with less Ge atomic composition. On the other hand, the various band alignments can be realized with controlling the state of the strain in SiGe layers. Compressively-strained- $\text{Si}_{1-x}\text{Ge}_x$  ( $x \lesssim 0.4$ ) quantum wells (QWs) on Si substrates show the type-I character, i.e., the narrower  $\text{Si}_{1-x}\text{Ge}_x$  bandgap falls within the wider Si bandgap where the valence band offset,  $\Delta E_v$ , is much larger than the conduction band offset,  $\Delta E_c$ . Tensilely-strained-Si QWs on relaxed  $\text{Si}_{1-x}\text{Ge}_x$  layers show the totally different character. The conduction band edge of the  $\text{Si}_{1-x}\text{Ge}_x$  lies higher than that of the Si, i.e., the type-II QWs can be obtained where electrons are effectively confined in the Si QWs. Knowledge of the

bandgap of the strained-Si<sub>1-x</sub>Ge<sub>x</sub> layers and the strain-dependent band alignment, when combined with the advanced growth technique such as MBE, has allowed us to obtain a number of interesting electrical and optical phenomena based on the Si<sub>1-x</sub>Ge<sub>x</sub>/Si heterostructures. Extraordinarily high electron mobility has been obtained in n-type modulation doped strained-Si/relaxed-Si<sub>1-x</sub>Ge<sub>x</sub> heterostructures [3]-[6]. Two-dimensional hole gases with high mobility have been realized in p-type modulation doped strained-SiGe/Si heterostructures [7]-[9], and SiGe hetero bipolar transistor (HBT) with  $f_t$  and  $f_{max}$  value in excess of 100GHz has been demonstrated [10]. Far-infrared detectors can be fabricated by utilizing intersubband transitions in the both valence [11][12] and conduction [13] bands, and its normal incident operation is also possible by utilizing inter valence band transitions [14]. Photoluminescence (PL) from strained-SiGe/Si QWs has been observed in the entire range of the alloy composition [15][16] and room-temperature-operation of light-emitting-diode has been demonstrated [17][18]. These results clearly show the potential of SiGe/Si heterostructures for application to Si-based optoelectronics.

The purpose of this research is to explore novel heterostructures based on the SiGe/Si for further improvements of optical properties. In fact, most of pioneering studies on PL from SiGe have been devoted to strained-Si<sub>1-x</sub>Ge<sub>x</sub>/Si QWs on Si substrates as will be introduced in chapter 2. In the strained-SiGe/Si QWs, the band offset is almost consumed at valence band side which allows only holes to be effectively confined in QWs. Based on the "band-engineering" concept to control the state of the strain, it is considered that there exists more sophisticated heterostructures which can drastically improve luminescence efficiency.

## 1.2 Organization

This thesis is organized as follows.

Chapter 2 is intended to give an overview of the strained-SiGe/Si heterostructures. The topics include the modification of the band structure by strain which originates from the lattice mismatch between Si and Ge. The band structure of strained-SiGe is totally

different from that of unstrained-bulk. The degenerate conduction and valence bands split and the bandgap is drastically reduced. The band alignment of SiGe/Si is explained in terms of the "model-solid" theory. The detail of MBE growth is described focusing on the difference between gas-source MBE and solid-source MBE. The kinetics of Ge surface segregation, which is inherent to solid-source MBE, is introduced. A method to create abrupt Si/Ge interface, "segregant assisted growth", is also introduced. The method utilizes atoms which show strong segregation tendency in order to suppress the surface segregation of Ge atoms. Chapter 2 also summarizes the pioneering work on PL of unstrained and strained SiGe alloy and QWs which was performed in the late 1980's to the early 1990's.

Chapter 3 deals with newly developed semiconductor heterostructures, neighboring confinement structure (NCS). NCS is exploited to realize effective confinement of both electrons and holes in SiGe/Si system. NCS consists of a pair of type-II neighboring layers to confine electrons and holes sandwiched between barrier layers. NCS can be realized by growing a pair of a tensilely strained-Si layer and a compressively strained-Si<sub>1-y</sub>Ge<sub>y</sub> layer between completely relaxed Si<sub>1-x</sub>Ge<sub>x</sub> ( $y > x$ ) layers. The strained-Si and the strained-Si<sub>1-y</sub>Ge<sub>y</sub> layers act as QWs for electrons and holes, respectively. Detailed PL studies on NCS are given, including observation of intense PL with strongly enhanced NP transitions and investigation of its origin by time-resolved PL spectroscopy.

Chapter 4 describes fabrication and optical properties of SiGe/Si quantum wires (QWRs) on V-groove patterned Si substrates. PL from the SiGe/Si QWRs at the bottom of the V-groove is clearly observed and it is found that the strain inside the V-groove leads to the increase of the bandgap. Dynamics of exciton diffusion in V-groove patterned substrates is also investigated. In addition, optical anisotropy which is specific to the wire geometry is observed in electroluminescence from the SiGe/Si QWRs selectively grown inside the V-groove.

Chapter 5 briefly introduces the other candidates for improvements of optical properties of Si-based heterostructures, especially low-dimensional structures based on strain-induced band structure. The first is an attempt to utilize inhomogeneous strain field

generated by Ge islands to locally modulate in-plane potential of the buried SiGe/Si QWs. Successful modulation of the potential is demonstrated by spectral red-shift in PL from SiGe/Si QWs with Ge islands. Also, a method to control the size and the position of spontaneously formed Ge islands is proposed. The method is to grow Ge islands on the cleaved-edge of strained multiple QWs which acts as a substrate with in-plane modulated lattice constant, which induce periodic strain to the epitaxial layer. The method is successfully applied to align Ge islands on the cleaved edge of SiGe/Si multiple QWs.

Finally, concluding remarks will be given in Chapter 6.

## 2. Strained-Si<sub>1-x</sub>Ge<sub>x</sub>/Si heterostructures : An overview

### 2.1 Band modification by SiGe/Si heterostructures

#### 2.1.1 Strains

The strains in pseudomorphically grown heterostructures are derived by minimization of the macroscopic elastic energy under the constraint that the *in-plane* lattice constant,  $a_{para}$ , is preserved throughout the heterostructures. For a system where  $h_1$  and  $h_2$  are the thicknesses of the unstrained materials which construct the heterostructures, following results are obtained:

$$a_{para} = \frac{a_1 G_1 h_1 + a_2 G_2 h_2}{G_1 h_1 + G_2 h_2} \quad (2.1)$$

$$a_{i, perp} = a_i \left\{ 1 - D_i \left( \frac{a_{para}}{a_i} - 1 \right) \right\} \quad (2.2)$$

$$\varepsilon_{i, para} = \frac{a_{para}}{a_i} - 1 \quad (2.3)$$

$$\varepsilon_{i, perp} = \frac{a_{i, perp}}{a_i} - 1 \quad (2.4)$$

where  $i$  denotes the material (1 or 2),  $a_i$  the equilibrium lattice constants,  $a_{i, perp}$ , the strained lattice constants perpendicular to the interface,  $\varepsilon$  is the component of the strain tensor, and  $G_i$  is the shear modulus,

$$G_i = 2 \left( c'_{11} + 2c'_{12} \right) \left( 1 - \frac{D^2}{2} \right) \quad (2.5)$$

where  $c'$  denotes the elastic constants of the constituent materials. It is noted that the constant  $D$  depends on the interface orientation:

$$D_{001} = 2 \frac{c_{12}}{c_{11}} \quad (2.6)$$

$$D_{110} = \frac{c_{11} + 3c_{12} - 2c_{44}}{c_{11} + c_{12} + 2c_{44}} \quad (2.7)$$

$$D_{111} = 2 \frac{c_{11} + 2c_{12} - 2c_{44}}{c_{11} + 2c_{12} + 4c_{44}} \quad (2.8)$$

An assumption that one of the materials is rigid leads to the fact that the *in-plane* lattice constant of the other material is the same with that of the rigid material as can be obtained from (2.1) when  $h_1/h_2 \rightarrow \infty$ . This corresponds to the case that a very thin layer is grown on a thick substrate with different lattice constant. In following discussions,  $z$  is defined as the growth direction parallel to the [001] and we assume that the substrate is rigid. In this case, the strain tensor has only diagonal components:

$$\epsilon_{xx} = \epsilon_{yy} = \epsilon \quad (2.9)$$

$$\epsilon_{zz} = -\frac{2c_{12}}{c_{11}} \epsilon \quad (2.10)$$

### 2.1.2 Valence band

The valence band edge of Si and Ge is three-fold degenerate in the absence of spin.

The inclusion of spin leads to six states which are split into a four folded state ( $J=3/2$ ) and a two-folded state ( $J=1/2$ ). The strain Hamiltonian,  $H_\epsilon$ , can be written as follows [19]:

$$H_\epsilon = a(\epsilon_{xx} + \epsilon_{yy} + \epsilon_{zz}) - 3b \left[ \left( L_x^2 - \frac{1}{3} L^2 \right) \epsilon_{xx} + c.p. \right] - \frac{6}{\sqrt{3}} d \left[ \{ L_x, L_y \} \epsilon_{xy} + c.p. \right] \quad (2.11)$$

where  $a$ , denotes the hydrostatic deformation potential,  $b$  and  $d$  are the shear deformation potentials for tetragonal and trigonal symmetry, respectively, and *c.p.* stands for cyclic permutation. By substituting (2.9) and (2.10) to (2.11), we get:

$$\begin{aligned} H_\epsilon &= a(\epsilon_{xx} + \epsilon_{yy} + \epsilon_{zz}) + 3b \left( \frac{1}{3} L^2 - L_z^2 \right) (\epsilon_{zz} - \epsilon_{xx}) \\ &= \delta E_H + \frac{3}{2} \delta E_{001} \left( \frac{1}{3} L^2 - L_z^2 \right) \end{aligned} \quad (2.12)$$

Here, we defined

$$\delta E_H = a(\epsilon_{xx} + \epsilon_{yy} + \epsilon_{zz}) \quad (2.13)$$

$$\delta E_{001} = 2b(\epsilon_{zz} - \epsilon_{xx}) \quad (2.14)$$

where  $\delta E_H$  denotes the hydrostatic component and gives rise to uniform shift, and  $\delta E_{001}$  is the uniaxial component and leads to splitting of degenerate energy bands.

The total perturbation Hamiltonian with including spin-orbit interaction can be written in the matrix form with the angular momentum basis. In the case of the [001] distortion, the 6x6 Hamiltonian breaks up into two 3x3 matrices as follows (note that the state ordering is  $|3/2, 3/2\rangle, |3/2, 1/2\rangle, |1/2, 1/2\rangle$ ):

$$\begin{pmatrix} \delta E_H + \frac{1}{3} \Delta_0 - \frac{1}{2} \delta E_{001} & 0 & 0 \\ 0 & \delta E_H + \frac{1}{3} \Delta_0 + \frac{1}{2} \delta E_{001} & -\frac{1}{\sqrt{2}} \delta E_{001} \\ 0 & -\frac{1}{\sqrt{2}} \delta E_{001} & \delta E_H - \frac{2}{3} \Delta_0 \end{pmatrix} \quad (2.15)$$

The Hamiltonian can be readily diagonalized and yields three eigenstates (each doubly degenerate) given by:

$$E_{v_2} = \delta E_H + \frac{1}{3} \Delta_0 - \frac{1}{2} \delta E_{001} \quad (2.16)$$

$$E_{v_1} = \delta E_H - \frac{1}{6} \Delta_0 + \frac{1}{4} \delta E_{001} + \frac{1}{2} \sqrt{\Delta_0^2 + \Delta_0 \delta E_{001} + \frac{9}{4} (\delta E_{001})^2} \quad (2.17)$$

$$E_{v_3} = \delta E_H - \frac{1}{6} \Delta_0 + \frac{1}{4} \delta E_{001} - \frac{1}{2} \sqrt{\Delta_0^2 + \Delta_0 \delta E_{001} + \frac{9}{4} (\delta E_{001})^2} \quad (2.18)$$

It is noted that the band  $v_2$  (heavy hole) is a pure  $|3/2, 3/2\rangle$  state, while  $v_1$  and  $v_3$  are mixtures of  $|3/2, 1/2\rangle$  and  $|1/2, 1/2\rangle$ .

### 2.1.3 Conduction band

The minima of the conduction band in Si are located along  $\Delta$  ([100] directions in the reciprocal space), while in Ge at L points, i.e., the zone boundary along the [111] directions. In the case of the unstrained-Si<sub>1-x</sub>Ge<sub>x</sub> alloy, the lowest conduction band changes from  $\Delta$  to L at  $x=0.85$  Ge composition.

The general description of the energy shift of the valley  $i$ ,  $\Delta E_i'$ , is

$$\Delta E_i' = (\bar{\Xi}_j \bar{1} + \bar{\Xi}_i \{\hat{\alpha}_i \hat{\alpha}_i\}) : \bar{\epsilon} \quad (2.19)$$

where  $\bar{1}$  is the unit tensor,  $\hat{\alpha}_i$  is a unit vector parallel to the  $\mathbf{k}$  vector of valley  $i$ , and  $\{\}$  is a dyadic product [20]. The uniform shift of the conduction bands due to the hydrostatic components can be expressed as

$$\Delta E_{c,av} = \left\{ \bar{\Xi}_j + \frac{1}{3} \bar{\Xi}_i \right\} \bar{1} : \bar{\epsilon} \quad (2.20)$$

The quantity  $(\bar{\Xi}_j + \frac{1}{3} \bar{\Xi}_i)$  corresponds to the hydrostatic deformation potential  $a_i$  for the conduction band. Under the [001] uniaxial stress, the bands along [100] and [010] split off from the one along [001]. The energy splitting with respect to the average is given by

$$\Delta E_c^{001} = \frac{2}{3} \bar{\Xi}_a^{\Delta} (\epsilon_{zz} - \epsilon_{xx}) \quad (2.21)$$

$$\Delta E_c^{100,010} = -\frac{1}{3} \bar{\Xi}_a^{\Delta} (\epsilon_{zz} - \epsilon_{xx}) \quad (2.22)$$

In the case of the compressive strain, the conduction band minima are fourfold degenerate, while in the case of the tensile strain, the minima are twofold degenerate. As can be intuitively understood, conduction bands at L does not split by the [001] uniaxial stress.

### 2.1.4 Bandgap

The indirect bandgap of the unstrained-Si<sub>1-x</sub>Ge<sub>x</sub> alloy was first determined by Braunsstein *et al.* by absorption measurements [21]. Weber and Alonso systematically investigated the indirect bandgap by photoluminescence spectroscopy for liquid-phase-epitaxy grown Si<sub>1-x</sub>Ge<sub>x</sub> alloys [22]. They obtained the following quadratic expressions which represent the free-excitonic bandgaps of the Si<sub>1-x</sub>Ge<sub>x</sub> alloys:

$$E_g^{(s)}(x) = 1.155 - 0.43x + 0.0206x^2 \quad (2.23)$$

$$E_g^{(l)}(x) = 2.017 - 1.27x \quad (2.24)$$

It is noted that the lowest lying conduction bands change from  $\Delta(6)$  to L(4) at  $x=0.85$ .

The indirect bandgap of the strained-Si<sub>1-x</sub>Ge<sub>x</sub> alloy can be calculated with strain-induced uniform shifts and splitting of the degenerated bands. Figure 2-1 shows Ge composition dependence of the calculated bandgap of the strained-Si<sub>1-x</sub>Ge<sub>x</sub> alloy in comparison with the bulk. It can be seen that the bandgap is drastically reduced by introducing the strain. Experimental data for the strained-Si<sub>1-x</sub>Ge<sub>x</sub> alloys are also available for limited Ge composition range  $x < 0.22$ . Robbins *et al.* derived the following quadratic expression for the bandgap of compressively-strained-Si<sub>1-x</sub>Ge<sub>x</sub> alloys by fitting

experimental data obtained by PL measurements with considering composition-dependent exciton binding energy [23]:

$$E_g(x) = 1.17 - 0.896x + 0.396x^2 \quad (2.25)$$

### 2.1.5 Band alignment

When we grow semiconductor heterostructures, discontinuity takes place in the valence and conduction bands. As discussed in 2.2.3 and 2.2.4, the hydrostatic component of the strain tensor produces the uniform shifts of the band, and the uniaxial strain leads to the splitting of the degenerate bands. These effects significantly affect the band alignment of the semiconductor heterostructures with large amount of the lattice mismatch, such as  $\text{Si}_{1-x}\text{Ge}_x/\text{Si}_{1-y}\text{Ge}_y$ . In other words, various kinds of band alignments can be realized in  $\text{Si}_{1-x}\text{Ge}_x/\text{Si}_{1-y}\text{Ge}_y$  heterostructures owing to the strain effects.

Van de Walle *et al.* developed the "model solid theory" which directly predicts the band alignment of semiconductor heterostructures [24]. In their theory, the strain-induced band shifts and splittings are separately treated from the line-up problem. They regarded the band offsets as linear quantities, which can be obtained as differences between reference values of the constituent semiconductors. The reference value corresponds to the average of the valence band position. It is noted that the absolute values of the reference level do not have physical meaning, and the difference between the two materials is of importance, i.e., it gives the band offset between unstrained materials. By taking the strain effects and the bandgap of the constituent materials into consideration, the band alignment can be readily calculated with the model solid theory. Many experiments support the validity of this theory [25]-[27]. Figure 2-2 shows the band alignment of strained- $\text{Si}_{1-x}\text{Ge}_x$  on unstrained- $\text{Si}_{1-y}\text{Ge}_y$  ( $y=0,0.5$ ) calculated with the model solid theory. The band parameters used for the calculations are listed in Table 2-1. It can be seen that the strained- $\text{Si}_{1-x}\text{Ge}_x$  quantum wells (QWs) on Si substrates show type-I character with low Ge composition, and change to type-II character with increasing  $x$  though the band offset at the conduction band is small. In the case of  $y=0.5$ , it can be

seen that the conduction band edge of the tensilely-strained-Si lies lower than that of the  $\text{Si}_{0.5}\text{Ge}_{0.5}$ , i.e., type-II strained-Si QWs can be formed by using relaxed- $\text{Si}_{1-y}\text{Ge}_y$  buffer layers. As is clarified, by utilizing the strain, various kinds of band alignment can be realized in  $\text{Si}_{1-x}\text{Ge}_x/\text{Si}$  system.

TABLE 2-1 Values of deformation potentials, spin-orbit splittings, elastic constants, D for different orientations, and lattice constants for Si and Ge. Linear interpolations were used for SiGe alloys.

	Si	Ge
$\left(\Xi_d + \frac{1}{3}\Xi_u - a_v\right)^\Delta$ (eV)	1.72	1.31
$b$ (eV)	-2.35	-2.55
$d$ (eV)	-5.32	-5.50
$\Xi_u^\Delta$ (eV)	9.16	9.42
$\Delta_0$ (eV)	0.04	0.30
$c_{11}$	1.675	1.315
$c_{12}$	0.650	0.494
$c_{44}$	0.801	0.684
$D^{001}$	0.776	0.551
$D^{110}$	0.515	0.450
$D^{111}$	0.444	0.371
$a$ (Å)	5.43	5.65

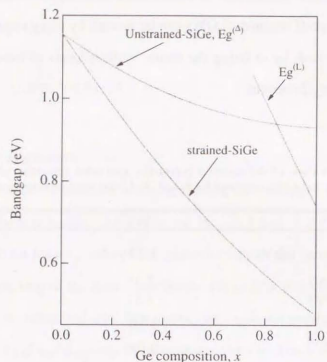


Fig. 2-1 Fundamental indirect bandgap of pseudomorphically strained SiGe alloys on Si (100) in comparison with the unstrained bulk alloy.

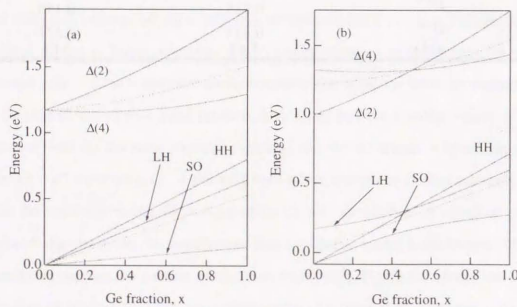


Fig. 2-2 Calculated electronic band structure of pseudomorphically strained SiGe alloys on (a) Si(100) and (b) relaxed-Si<sub>0.5</sub>Ge<sub>0.5</sub>.

## 2.2 Epitaxial growth of SiGe/Si by Molecular Beam Epitaxy (MBE)

### 2.2.1 Solid-source MBE

MBE is a growth technique which involves the generation of fluxes (molecular beam) of source materials and their interaction with a substrate under ultrahigh vacuum (UHV) environment. The molecular beam is provided by a heated material in a crucible which is kept at a proper temperature such that its vapor pressure is sufficiently high to generate the required flux. For the material with high melting point such as Si, an electron beam is alternatively used as the heating source. Close control of the flux is performed by maintaining the temperature of crucibles for effusion cells, and by keeping the emission current for electron beam evaporators. Under UHV environment, it takes more than  $10^5$  seconds before the residual gas impinges to all the surface sites of the substrate. Therefore, we can decrease the growth rate to a few Å/sec. and precise control of film thickness can be obtained. Abrupt compositional transition can also be obtained by rapidly opening(closing) mechanical shutters, because the interaction between the residual gas and molecular beam can be negligible. Various kinds of "in situ" characterizations of the epitaxial layer can be used owing to UHV environment. Most of commercially available MBE systems are equipped with representative diagnostic instruments such as reflective high energy electron diffraction (RHEED), Auger electron spectroscopy (AES), x-ray photoelectron spectroscopy (XPS), quadruple mass spectrometer (QMS) and so on.

### 2.2.2 Gas-source MBE

Gas-source MBE proceeds with adsorption of the dissociated hydride source to the surface dangling bonds, subsequent desorption of hydrogen at the growth front, and reappearance of the dangling bonds [28]-[30]. Owing to this mechanism, temperature dependence of the growth rate is not simple in contrast to the solid-source MBE. Figure 2-3 (a) shows a typical temperature dependence of the growth rate of Si on Si(100) substrates with a constant disilane flow rate of 2.5 sccm. It can be seen that the growth rate increases with increasing temperature, and saturates at higher temperatures. The former is "reaction-limited" regime where the desorption of the surface hydrogen is not

enough and a part of decomposed gases cannot find dangling bonds. The activation energy deduced from the Arrhenius plot is in good agreement with the Si-H bond energy. The latter is known as "adsorption-limited" or "supply-limited" regime where the growth front is almost free from hydrogen due to the enhanced desorption at higher temperatures. The growth rate is limited by the flow rate of the source-gas and does not depend on temperature. The existence of the two regimes is also illustrated in Fig. 2-3 (b) where the flow rate dependence of the growth rate is shown at different two temperatures. At 620 °C, the growth rate is independent of the flow rate ("reaction-limited"). On the other hand, the growth rate linearly increases with increasing flow rate at 740 °C ("adsorption-limited").

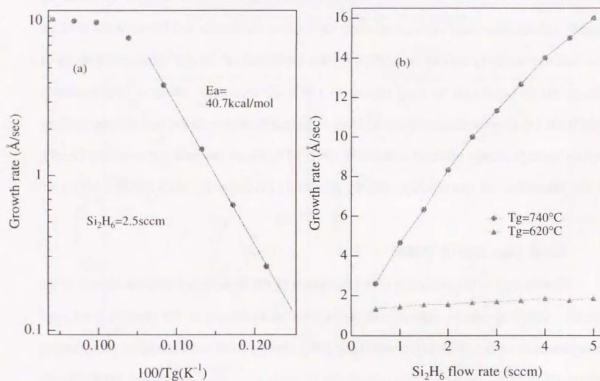


Fig. 2-3 Growth rate of Si on Si(100) as a function of (a) temperature with a constant disilane flow rate of 2.5sccm and (b) flow rate at fixed temperature of 740 and 620 °C.

### 2.2.3 Ge surface segregation

Interfacial mixing of Si/SiGe due to Ge surface segregation is one of the most serious problems in obtaining the desired quantum wells and/or superlattices. This phenomenon has been observed by several groups using various surface analytical techniques. Eberl *et al.* showed the existence of considerable intermixing between Si and Ge atoms on topmost layer during growth by AES [31]. Iyer *et al.* observed the asymmetric mixing of Ge atoms into Si overlayer using Raman spectroscopy and medium energy ion scattering (MEIS) [32]. Zalm *et al.* studied the interfacial quality of Si/SiGe by means of secondary ion mass spectrometry (SIMS) [33]. X-ray photoelectron spectroscopy (XPS) is also useful technique to detect the existence of Ge surface segregation as reported by Fujita *et al.* [34]. Comprehensive treatment of this phenomenon taking into account the alloy-specific effect of "self-limitation" associated with the atom site swap was first addressed by Fukatsu *et al.* [35]-[37]. This scheme incorporates the atomistic arrangement and individual atom swap between the surface and subsurface sites. Figure 2-4 shows energy diagram of surface and subsurface sites, where  $E_a$  is the kinetic barrier,  $E_b$  is the Gibbsian heat of segregation, and  $E_d$  is the desorption energy. As shown in this figure, Ge atoms lower surface free energy by segregating to the growth front. Earlier theoretical works based on such a two state exchange scheme [38][39] have already succeeded in explaining the exponential decay of Ge atoms toward surface, corresponding to the dilute limit of atomic concentration of segregating material. However, they failed to describe the atomic concentration dependence of Ge profile, particularly the occurrence of non-exponential decay for a high concentration ( $n_{Ge} > 0.1$  ML). The initial steep is due to the large probability of interchange between surface and subsurface Ge atoms where the Ge atomic concentration is high. This process is called as "self-limitation" since Ge atoms control Ge segregation by themselves.

Following rate equations are proposed to describe Ge surface segregation

$$\frac{dn_1}{dt} = -2f_0 \exp\left(-\frac{E_d}{k_B T}\right)n_1(1-n_2) + 2f_0 \exp\left(-\frac{E_d + E_b}{k_B T}\right)n_2(1-n_1) \quad (2.25)$$

$$\frac{dn_2}{dt} = -2f_0 \exp\left(-\frac{E_a + E_b}{k_B T}\right) n_2 (1 - n_1) + 2f_0 \exp\left(-\frac{E_c}{k_B T}\right) n_1 (1 - n_2) \quad (2.26)$$

where  $n_1$  and  $n_2$  are the Ge atomic coverage of the subsurface and surface, respectively,  $f_0$  denotes the jump trial frequency,  $k_B$  is the Boltzman's constant, and  $T$  is the growth temperature. Ge desorption energy can be negligible at the MBE growth temperature. The factors  $(1 - n_i)$  represent the self-limiting process.

Figure 2-5 shows normalized XPS signal intensity as a function of MBE grown Si overlayer thickness. After 3ML of Ge deposition, Si overlayer was grown using electron beam evaporator at 500 °C. Open circles represent the experimental data, where Ge 2p<sup>3/2</sup> core level emissions are normalized by Si 2p<sup>3/2</sup> ones. Non-exponential decay suggests the existence of segregating Ge atoms. Solid line is the result of a numerical calculation taking three different Ge contributions into consideration as follows:

$$\frac{I(n)}{I(0)} = \frac{\theta}{3} n_2^{(s)}(t_m) + \frac{\theta}{3} \sum_{i=1}^n n_1^{(i)}(t_m) \exp\left(-\frac{(n-i)d}{\lambda_{Ge}}\right) + \frac{3-\theta}{3} \exp\left(-\frac{nd}{\lambda_{Ge}}\right) \quad (2.27)$$

where the first term comes from the surface Ge atoms, the second term is the contribution of incorporated Ge atoms into Si overlayer, and the last term is from the Ge atoms staying at the initial site.  $I(n)$  represents the photoelectron intensity with  $n$  monolayer of overgrowing Si,  $\theta$  is the amount of segregating Ge atoms,  $t_m$  is the time for one monolayer growth,  $d$  is the one monolayer length of Si, and  $\lambda_{Ge}$  is the decay length of Ge 2p<sup>3/2</sup> photoelectron. Numerical calculation is in good agreement with the experimental data, demonstrating the validity of the treatment of Ge surface segregation.

#### 2.2.4 Segregant Assisted Growth

Ge surface segregation is unfavorable in order to achieve abrupt heterointerfaces. As a method to suppress the Ge surface segregation and to realize abrupt Si/SiGe interfaces, Copel *et al.* demonstrated a growth technique where energetics of growth is

altered using a "surfactant", and showed successful reduction of islanding formation and interfacial mixing using As surfactant layer [40]. In order to overcome the difficulty in controlling the As flux, Fujita *et al.* used submonolayer of Sb as a surfactant, and demonstrated the suppression of surface segregation of Ge atoms and formation of Si/Ge superlattices with abrupt interfaces using XPS and SIMS [34]. They named this growth technique as "segregant assisted growth (SAG)" after the tendency of Sb which shows strong segregation in Si [35]. Usami *et al.* applied SAG technique to grow strained-Si<sub>0.8</sub>Ge<sub>0.2</sub>/Si SQWs with well width of 30 Å by using 0.75 monolayers of Sb [41]. They demonstrated that the spectral blue-shift induced by potential distortion due to the Ge surface segregation can be successfully removed by SAG as shown in Fig.2-6. Sakamoto *et al.* showed that Bi can be also useful to produce abrupt Si/Ge interfaces, and found that the incorporation of Bi is less than the detection limit of SIMS ( $5 \times 10^{16} \text{cm}^{-3}$ ) in contrast to Sb which yields a doping level of  $\approx 10^{18} \text{cm}^{-3}$  [42]. Ohta *et al.* [43] and Nakagawa *et al.* [44] investigated the effects of atomic hydrogen on Si/Ge interface formation, and demonstrated that the Ge surface segregation can be suppressed with atomic hydrogen. This can be closely connected with the fact that the segregation length of Ge atoms grown by gas-source MBE is much shorter than that grown by solid-source MBE, since the presence of hydrogen at the growth front is inherent feature of gas-source MBE. Reduction of the surface migration of Ge atoms by atomic hydrogen is also demonstrated by Sakai *et al.* [45]. They showed that the atomic hydrogen suppresses the Ge island formation by high-resolution transmission electron microscopy (TEM), and Ebuchi *et al.* showed that the (311) facet length developed on V-grooved Si substrates is drastically reduced in the presence of atomic hydrogen [46].

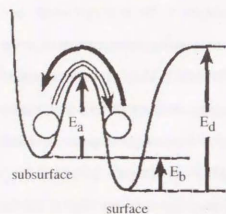


Fig.2-4 Schematic of energy diagram of exchange model of Ge segregation proposed by Fukatsu *et al.* [38]

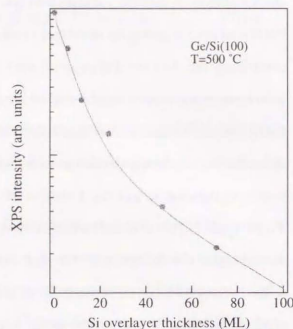


Fig.2-5 Ge  $2p^{3/2}$  photoelectron as a function of Si overlayer thickness grown by solid-source MBE.

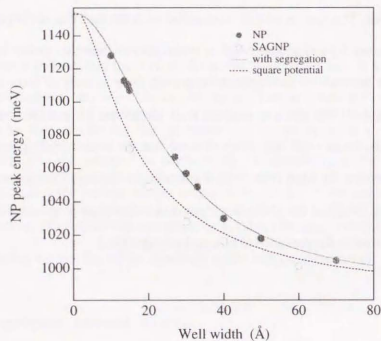


Fig.2-6 PL peak energies of strained- $\text{Si}_{1-x}\text{Ge}_x/\text{Si}$  single quantum wells grown by solid-source MBE with (open circles) and without (solid circles) Sb adlayer.

### 2.3 Photoluminescence of strained $\text{Si}_{1-x}\text{Ge}_x/\text{Si}$ quantum wells

Si has not been recognized as a promising candidate of light emitting materials for a long time because of poor recombination probability due to its inherent indirect nature of band structure. However, the pioneering works of PL from SiGe bulk and quantum wells clearly demonstrated their potential as a light-emitting material. Now, optical properties of  $\text{Si}_{1-x}\text{Ge}_x/\text{Si}$  heterostructures are being extensively studied motivated by a desire to implicate them to Si-based optoelectronic device applications. Followings are some representative works on PL from SiGe reported in the late 1980's to the early 1990's.

To the best of our knowledge, the first systematic study on PL from relaxed SiGe bulk was reported by Weber and Alonso [22]. They prepared relaxed SiGe alloy with various Ge composition by liquid phase epitaxy and performed PL measurements. They clearly observed near band-edge transitions including NP transition and its phonon replicas. The Ge composition dependence of the relative NP intensity was explained in terms of alloy disordering. The  $\Delta$  to L changeover of the conduction band character was also observed. Terashima *et al.* reported near band-edge PL from strained- $\text{Si}_{1-x}\text{Ge}_x$  ( $x=0.04, 0.15$ ) thin films grown by solid-source MBE on Si (100) substrates [47]. Strain-induced reduction of the band gap was clearly demonstrated. Noël *et al.* observed systematic PL energy shift with varying Ge alloy composition of strained-SiGe/Si MQWs grown by solid-source MBE [48]. However, the peak energy was consistently  $\approx 100\text{meV}$  lower than the strained band gap of the alloy and the full width of half maximum of the PL peak was quite broad. They assigned the origin of the deep-level luminescence as Ge platelet formed during growth [49]. This "deep-level" luminescence was also reported by other groups using solid-source MBE [50][51]. However, it was found that it can be removed by optimizing growth conditions and growing high-quality materials[52][53]. The first observation of band-edge PL from strained SiGe/Si QWs was reported by Sturm *et al.* [54] who used rapid thermal chemical vapor deposition technique. After their report, various groups succeeded in growing luminescent strained-SiGe/Si QWs, and their basic properties were disclosed, including the quantum size effect with well width variation [55]-[57], the effect of the Ge surface segregation on the quantized energy [58],

the suppression of the Ge surface segregation with Sb adlayer [41], the Ge interdiffusion induced by post-growth annealing [59][60], the interwell coupling through tunneling barriers [61], the kinetics of photogenerated carriers [62][63], the optimization of the structure and the observation of room-temperature-PL [64], and so on.

### 3. Neighboring Confinement Structure

#### 3.1 Introduction

As shown in the previous chapter, most of earlier reports on PL from SiGe/Si heterostructures have been focused on strained-SiGe/unstrained-Si QWs. In strained-SiGe/Si QWs, the band offset is almost consumed at valence band side which allows only holes to be effectively confined in QWs. In order to overcome this problem, it is effective to utilize a relaxed SiGe buffer layer as a pseudosubstrate. Since the lattice constant of relaxed-SiGe is larger than that of Si, epitaxial growth of a thin Si layer results in biaxial tensile strain in the epitaxial Si layer. In this case, six-folded conduction bands  $\Delta(6)$  split into  $\Delta(4)$  and  $\Delta(2)$ , and the  $\Delta(2)$  conduction bands lie below the  $\Delta(4)$  unlike the compressively strained-layer. The model-solid theory predicts that the  $\Delta(2)$  conduction bands of strained-Si lie  $\approx 106\text{meV}$  below those of relaxed  $\text{Si}_{0.82}\text{Ge}_{0.18}$ . Therefore, it can be possible to confine electrons with a high potential barrier in tensilely strained-Si/relaxed-SiGe QWs. Nayak *et al.* prepared 5-stacked tensilely strained-Si/unstrained- $\text{Si}_{0.82}\text{Ge}_{0.18}$  QWs with various Si well width by gas-source MBE and demonstrated the first clear observation of excitonic PL and systematic spectral shift due to the quantum confinement effect as shown in Fig.3-1 [65]. However, the PL intensity is limited to be low since the system constitutes type-II band alignment which spatially separates electrons and holes in addition to the indirect band nature in k-space, and no special structure to confine holes was considered. From a practical point of view, it is desirable to confine both electrons and holes with high potential barriers.

In order to realize effective confinement both electrons and holes in SiGe/Si system, we exploit a new class of semiconductor heterostructures, Neighboring Confinement Structure (NCS), as a method to enhance radiative recombination of indirect semiconductors. A typical band diagram of Si-based NCS is illustrated in Fig.3-2, where a pair of type-II neighboring layers to confine electrons and holes are sandwiched by barrier layers. NCS can be realized in the SiGe/Si system by sandwiching a pair of a tensilely strained-Si layer and a compressively strained- $\text{Si}_{1-y}\text{Ge}_y$  layer between

completely relaxed  $\text{Si}_{1-x}\text{Ge}_x$  ( $y>x$ ) layers. It is noted that  $\Delta(2)$  electrons and heavy holes construct NCS band structure. The strained-Si and the strained- $\text{Si}_{1-y}\text{Ge}_y$  layers act as QWs for electrons and holes, respectively. In spite of the indirect band structure in real- and  $k$ -spaces, radiative recombination is expected to be enhanced since the spatial overlap of wavefunctions of electrons and holes can be comparable to that of type-I QWs due to the penetration of wavefunctions by optimization of mutual layer thickness. In fact, it has been reported that even a single pair of GaP/AIP-based NCS surpasses GaP/AIP superlattices with hundreds periods in PL efficiency [66], indicating that the Si-based NCS is also promising as a candidate to enhance luminescence efficiency.

Originally, a similar band structure has been proposed in AlGaAs/GaAs system [67], where a pair of GaAs/AlAs was cladded with AlGaAs barriers. In this case, holes are confined in the GaAs layer, and  $\Gamma$ -electrons and X-electrons are confined in the GaAs layer and the AlAs layer, respectively. The structure has been used for fundamental study of the effect of  $\Gamma$ -X mixing on the optical properties since it is possible to control the separation of  $\Gamma$ -electrons and X-electrons by applying an external electric field. In addition, the long-lived X electrons were used for the carrier sources for the resonant injections to the localized  $\Gamma$ -states formed by the microscopic interface roughness, and lead to the first observation of ultranarrow PL from a single quantum dot [68].

This chapter is organized as follows. Following to this introductory section, details of our experiments are given in section 3.2. Section 3.3 is devoted to describe the general feature of PL spectra of NCS, addressing that NP transitions are dramatically enhanced. Section 3.4 describes the origin of the enhancement of NP transitions which was closely investigated by post-growth annealing of the samples and time-resolved PL spectroscopy. An attempt to increase the critical temperature of the NP enhancement and a preliminary experiment to implicate NCS to light-emitting-diode are given in Section 3.5. A summary of this chapter is given in 3.6.

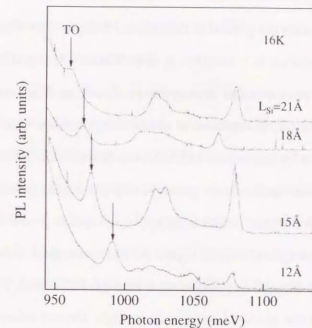


Fig.3-1 PL spectra of type-II strained-Si quantum wells with various well width of 12 to 21Å grown by gas-source MBE. Arrows show PL with TO phonon assistance from excitons confined in strained-Si wells. Quantum confinement effect can be clearly seen.

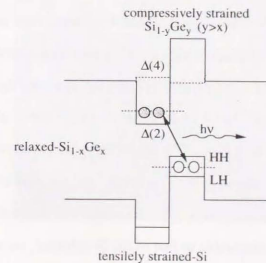


Fig.3-2 Schematic band structure of Si-based NCS. Electrons and holes are confined in tensilely strained-Si and compressively strained-SiGe, respectively.

### 3.2 Experiment

Basic requirement for the growth of the strained-Si layer is to obtain a good quality relaxed SiGe buffer layer on Si substrates. It is well known that gradual change of Ge composition is useful to reduce the density of the threading dislocations [69]. In this study, step-graded technique is exploited to obtain a high-quality SiGe buffer layer. All the samples were grown by gas-source MBE (Daido-Hoxan VCE S2020) using disilane ( $\text{Si}_2\text{H}_6$ ) and germane ( $\text{GeH}_4$ ) as source gases. A step-graded  $\text{Si}_{1-x}\text{Ge}_x$  layer with  $x$  of 0 to 0.18 in 9 steps capped with a uniform  $\text{Si}_{0.82}\text{Ge}_{0.18}$  layer is grown at  $800^\circ\text{C}$  to fully relax the strain inside the epitaxial layer. Figure 3-3 shows a typical cross-sectional bright field TEM image of a  $\text{Si}_{0.82}\text{Ge}_{0.18}$  layer with step-graded layers. It is seen that the dislocation density in the graded layers is quite high. On the other hand, threading dislocations can be hardly seen in the uniform relaxed-layer. This evidences that the step-graded layers play a role as cut-filters for threading dislocations. Figure 3-4 shows a sputter depth profile of  $^{30}\text{Si}$  and  $^{74}\text{Ge}$  ion counts of the step graded layers. Nine plateau, which are consistent with step numbers of the graded layer, can be clearly seen, showing the gradual change of the Ge alloy composition. The width of the plateau is seen to increase with decreasing Ge composition. Since the growth time and the flow rate of  $\text{Si}_2\text{H}_6$  were fixed during each step, the addition of  $\text{GeH}_4$  is considered to bring reduction of the growth rate. Figure 3-5 shows an x-ray rocking curve of the SiGe buffer layer obtained by using a Ge single crystal analyzer as an exit slit which allows us to obtain a curve with angular resolution of 12 sec (Philips Expert MRD). The sharp peak labeled Si corresponds to the (400) reflection of the Si substrate, and the peak at lower angle comes from the uniform and the graded SiGe layer. The width of the peak from the topmost SiGe layer is found to be comparable to that of the Si substrate, showing the uniformity of the SiGe buffer layer is excellent. On this buffer layer, a pair of tensilely strained-Si layer and compressively strained- $\text{Si}_{0.64}\text{Ge}_{0.36}$  (or pure-Ge) layers is grown as QWs for electrons and holes, respectively. The sample is completed with  $\approx 1\mu\text{m}$   $\text{Si}_{0.82}\text{Ge}_{0.18}$  cap layer for PL measurements. The thickness of the cap layer was chosen to isolate the active layers from the nonradiative surface states. Growth temperature for the strained-

layers was lowered to  $700^\circ\text{C}$  in order to avoid strain relaxation and interdiffusion of Ge atoms. Post growth annealing was performed in UHV environment for a part of samples to investigate the effect on PL properties.

Continuous-wave (CW) PL spectra were recorded using a standard lock-in technique with a multi-line argon ion laser as an excitation source and a liquid-nitrogen-cooled Ge photodetector (North-Coast EO-817L). Time-resolved PL was measured by the time-correlated photon counting method with an infrared-sensitive photomultiplier (Hamamatsu R5509-71 or R3236). The second harmonics of CW mode-locked yttrium-lithium-fluoride (YLF) laser pulses were used for the synchronous pumping of the dye laser and provided 5-ps pulses with repetition of 754 kHz at wavelength of 630 nm.

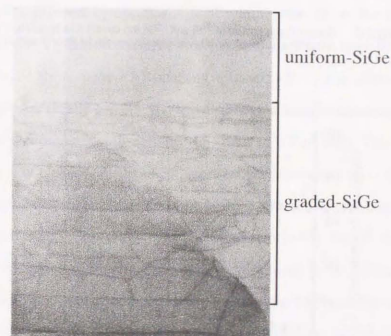


Fig. 3-3 A typical cross-sectional TEM image of a relaxed-SiGe layer with step-graded layers.

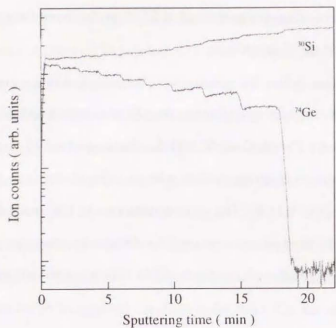
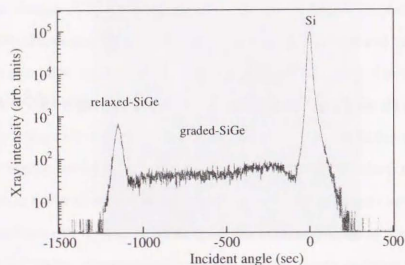


Fig.3-4 Sputter depth profile of  $^{30}\text{Si}$  and  $^{74}\text{Ge}$  ion counts as a function of sputtering time. Step-like change of Ge alloy compositions can be clearly seen.



4Fig.3-5 X-ray rocking curve of a relaxed SiGe buffer layer with a step-graded SiGe layer grown on Si(100) by gas-source MBE. The half width of the signal from the uniform layer is comparable to that of the Si substrate.

### 3.3 Photoluminescence: General feature

Figure 3-6 shows comparison of 18K PL spectra from different three samples, (a) 10Å-strained-Si QWs, (b) 10Å-strained-Si<sub>0.64</sub>Ge<sub>0.36</sub> QWs, and (c) 10Å-strained-Si/10Å-strained-Si<sub>0.64</sub>Ge<sub>0.36</sub> clad with Si<sub>0.82</sub>Ge<sub>0.18</sub> barriers (NCS). The sample (a) has type-II band alignment and  $\Delta(2)$ -electrons are confined in the Si well. On the other hand, the band alignment of the sample (b) is the same as that of strained-SiGe/Si QWs and the band offset is almost consumed at the valence band. In all the spectra, broad luminescence can be seen at 803 meV and 854 meV. They are assigned as well-known D1 and D2 lines [70], respectively, which originate from dislocation- and point defect-related emissions. In Fig.3-6 (a), at higher energies of dislocation-related PL, two NP and TO pairs can be seen as indicated by arrows. They are assigned as coming from excitons in the relaxed-SiGe buffer layer and the strained-Si well from the higher energy side, respectively, as confirmed by systematic well width variation. In the case of Si<sub>0.64</sub>Ge<sub>0.36</sub> QWs, NP and TO emissions can be clearly seen owing to the spatially-direct band configuration. In addition, relative NP intensity is found to be intense compared to type-II strained-Si QWs as seen in Fig.3-6 (b). This would be due to the enhanced alloy disordering since the excitons are confined in the Si<sub>0.64</sub>Ge<sub>0.36</sub> "alloy" layer. This seems to reflect the advantage of type-I band alignment, however, the band offset at conduction band is nearly zero and the confinement of electrons would be not enough. By employing NCS, spectral feature can be drastically changed as shown in Fig.3-6 (c). Intense radiative recombination, especially enhanced NP transition, is found in the NCS sample. It should be remarked that the structural difference between the NCS sample and the others is very small, that is, the insertion of only 10Å-Si<sub>0.64</sub>Ge<sub>0.36</sub> layer or 10Å-Si layer for sample (a) and (b), respectively. However, such a small structural difference can drastically induce band modification and bring improved spectral feature reflecting the effective confinement for both electrons and holes. The reason for strong enhancement of NP line and suppression of phonon replicas will be closely treated in the next section.

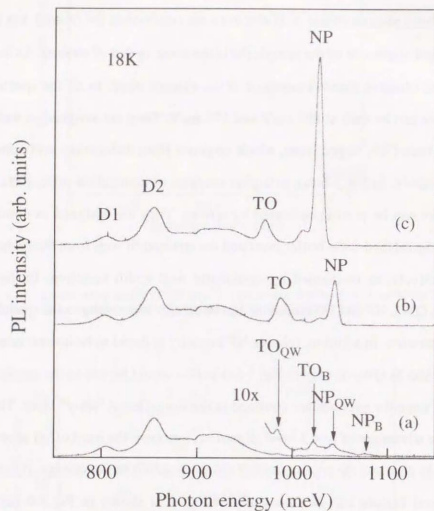


Fig.3-6 Comparison of PL spectra of (a) 10Å-stained Si type-II QW, (b) 10Å-stained-SiGe QW, and (c) NCS. Dramatic increase of PL intensity, especially NP transition, can be seen in NCS.

In order to confirm that the observed NP transition originates from expected recombinations, that is, electrons confined in the Si layer and holes confined in the  $\text{Si}_{0.64}\text{Ge}_{0.36}$  layer, a series of samples with different Si ( $\text{Si}_{0.64}\text{Ge}_{0.36}$ ) well widths were prepared while keeping the  $\text{Si}_{0.64}\text{Ge}_{0.36}$  (Si) width as 10Å. Figures 3-7 and 3-8 show Si width dependence of PL spectra and NP transition energy of NCS samples, respectively. It is noted that the transition energy was measured at 4.2K and 23K as shown in solid and open triangles, respectively. With increasing Si width from zero, the NP energy shifts toward higher energies first, reaches at maximum, and then decreases. The first increase of the NP energy can be understood by taking the band alignment at the valence band into account. The increase of the Si width leads to the increase of the effective barrier height for confined holes in the  $\text{Si}_{0.64}\text{Ge}_{0.36}$  layer, resulting in the spectral blue-shift. Further increase of Si width brings spectral shift to lower energies, showing that the Si layer acts as a QW for electrons. These results clearly show that the Si layer plays a different role for electrons and holes. Almost the same tendency was observed for another series of samples with different  $\text{Si}_{0.64}\text{Ge}_{0.36}$  width and fixed Si thickness. Therefore, it can unambiguously concluded that the observed intense NP line comes from the expected NCS transition.

The solid line in Fig.3-8 shows the calculated NP transition energies by using one-band effective mass approximation with band offset predicted by the model-solid theory and the other band parameters in literature. The tendency can be well reproduced with the calculation. It is noted, however, that the binding energy of excitons was estimated to be very large ( $\approx 30\text{meV}$ ) by fitting the calculated results to the experimental ones. In order to check that this value is reasonable for the Wannier excitons, we performed a rough estimation of the binding energy of excitons by standard variational method [71]. The calculation was carried out to minimize  $K_x + W_x$ , where  $K_x$  is kinetic energy of excitons;

$$K_x = \frac{\hbar^2}{2\mu_x} \int_0^\infty \rho \left( \frac{\partial \phi_0}{\partial \rho} \right)^2 d\rho \quad (3.1)$$

and  $W_x$  is the Coulomb energy term;

$$W_v = \int_{-\infty}^{\infty} u_v^2(z_r) dz_r \int_{-\infty}^{\infty} u_h^2(z_h) dz_h \int_0^{\infty} \rho \phi_0^2(\rho) V_v(\rho, z_r - z_h) d\rho \quad (3.2)$$

by using 1S nodeless trial wavefunction;

$$\phi_0(\rho) = \frac{1}{\lambda} \sqrt{\frac{2}{\pi}} \exp\left(-\frac{\rho}{\lambda}\right). \quad (3.3)$$

Here,  $\lambda$  is the variational parameter to be determined and is connected with Bohr radius of excitons. Figure 3-9 shows the Si width dependence of the calculated binding energy of Wannier excitons in NCS with fixed Si<sub>0.64</sub>Ge<sub>0.36</sub> width of 10Å. It is noted that the maximum binding energy is at most 22meV, and this value is largely different from the experimental value of 30meV. Therefore, the Wannier exciton picture is unlikely to be suitable for this case. The deviation would be compensated by considering additional binding energy due to exciton localization. This idea is also supported by the systematic increase of the NP energy at 23K compared to at 4.2K as shown in Fig.3-8. The increase of the temperature from 4.2K to 23K is considered to lead to partial delocalization of excitons and the shift of the peak energy to higher energies.

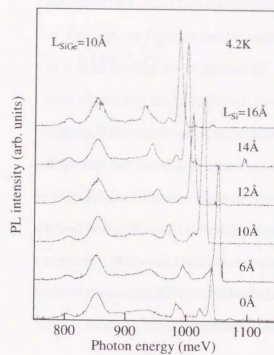


Fig.3-7 Si width dependence of PL spectra of NCS at 4.2K. Systematic peak shift reflecting the band structure of NCS can be seen.

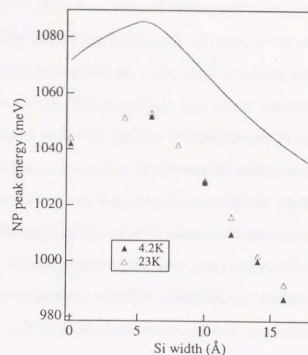


Fig.3-8 Si width dependence of NP peak energy at 4.2K and 23K. Solid-line represents the calculated result without the binding energy of excitons.

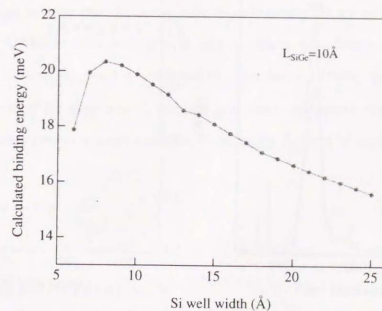


Fig.3-9 Si width dependence of binding energy of excitons in NCS with fixed SiGe width of 10Å calculated by a standard variational method.

### 3.4 The origin of the NP enhancement in NCS

In the previous section, the enhanced NP feature in NCS was presented and it was suggested that exciton localization is likely to occur at low temperatures. The localized excitons would be delocalized at a certain temperature where thermal energy  $k_B T$  is comparable to the depth of the localization potential. Therefore, it would be effective to measure temperature dependence of PL spectra to clarify the effect of exciton localization on PL feature. Figures 3-10 and 3-11 show typical temperature dependence of PL spectra and relative NP intensity to its TO phonon replica, respectively. It is noted that spectra in Fig.3-10 were normalized to give the same TO intensity. In addition to the roll-off of the integrated PL intensity with increasing temperature, the relative NP intensity was found to decrease. The former can be seen in most of excitonic transitions, however, the latter seems to be specific to NCS. This result suggests that the enhanced NP feature is closely connected with the exciton localization, in other words, dimensionality of excitons.

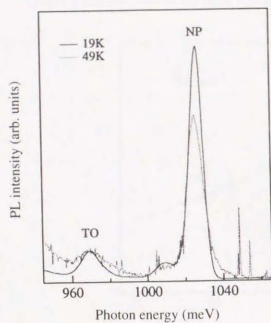


Fig.3-10 Comparison of PL spectra of NCS measured at 19K and 49K. Note that the spectra are normalized to give the same TO intensity.

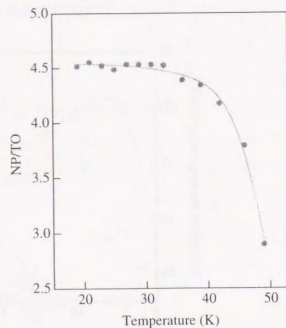


Fig.3-11 Typical temperature dependence of relative NP intensity of NCS. It can be seen that a rapid roll-off of the NP intensity takes place at a critical temperature.

Temperature dependence of radiative lifetime is known as an effective tool to probe the dimensionality of excitons [72][73]. In the case of two-dimensional excitons, the averaged radiative lifetime  $\tau(T)$  can be expressed as

$$\tau(T) \propto \tau_0 \frac{k_B T}{\Delta} \quad (3.4)$$

where  $\tau_0$  is the intrinsic lifetime of the exciton at  $k=0$ , and  $\Delta$  is the maximum kinetic energy of excitons which can decay radiatively. To deduce the above expression, we assumed that excitons with center-of-mass wave vector  $k < k_0$  can decay radiatively and their density of states is independent of energy as well known for two-dimensional excitons. In the case of localized (zero-dimensional) excitons, the density of states would be well approximated with  $\delta$ -like function resulting in temperature-independent radiative lifetime

$$\tau(T) = const. \quad (3.5)$$

Figure 3-12 shows temperature dependence of temporal profiles of NP transitions of NCS. It can be seen that the decay time monotonically decreases with increasing temperature. The observable decay time in the experiment,  $\tau_{exp}$ , does not directly reflect the radiative lifetime,  $\tau_R$ , since it is affected by nonradiative lifetime,  $\tau_{NR}$ , as suggested by rapid roll-off of the integrated PL intensity at higher temperatures. In the case that the observable decay time is monoexponential, PL intensity,  $I_{PL}$ , can be expressed as:

$$I_{PL}(t) \propto \frac{1}{\tau_R} \exp\left(-\frac{t}{\tau_{exp}}\right) \quad (3.6)$$

and time-integrated PL intensity,  $I_{tot}$ , is

$$I_{tot} = \int_0^{\infty} I_{PL}(t) dt \propto \frac{\tau_{exp}}{\tau_R} \quad (3.7)$$

Therefore, it is appropriate to exploit not  $\tau_{exp}$  but effective radiative lifetime,  $\tau_{eff}$ .

$$\tau_{eff} = \frac{\tau_{exp}}{I_{rel}} \quad (3.8)$$

to discuss dimensionality of excitons [74].

The effective lifetime is deduced by using temporal profiles and plotted as a function of temperature in Fig.3-13. It can be seen that the effective lifetime is almost independent of temperature at low temperatures, while above a critical temperature, it linearly increases with temperature. This shows that localization of excitons takes place at low temperatures, and delocalization occurs at  $\approx 40K$ . This behavior well correlates with temperature dependence of the relative NP intensity which showed a drastic reduction at  $\approx 40K$ , showing that the enhanced NP feature is closely connected with exciton localization.

The density of states of the localization center is considered to be  $\delta$ -like but finite, therefore it could be saturated with high excitation power. Figure 3-14 shows a typical excitation power dependence of PL spectra of NCS. The spectra under high excitations are totally different from those obtained at low excitations and they are likely to be deconvoluted into two components. In fact, the spectra are well reproduced by assuming that there exists two pairs of NP and TO. The peak at lower energy side, labeled L, shows almost no spectral shift, while the other peak, labeled F, gradually shifts to higher energies with increasing excitation power. In addition, relative NP intensity decreases with increasing excitation power. The procedure for the peak deconvolution was carried out for all the spectra, and the integrated PL intensity were plotted against excitation power in Fig.3-15. The behavior can be understood in terms of saturation of the localization center and subsequent band filling effect of free excitons in indirect materials. In other words, the saturation of localized excitons and the appearance of the higher energy peak are likely to reduce relative NP intensity.

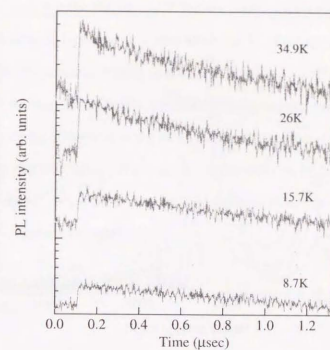


Fig.3-12 Temperature dependence of temporal profiles of NP transitions in NCS. The decay time monotonically decreases with increasing temperature.

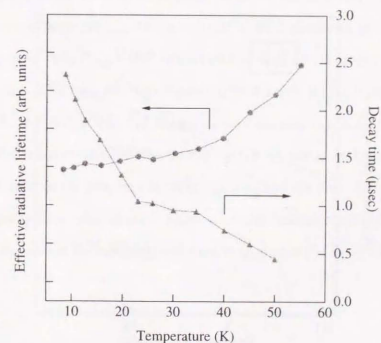


Fig.3-13 Temperature dependence of the effective radiative lifetime (left axis) deduced from the experimentally observed decay time (right axis) and time-integrated PL intensity.

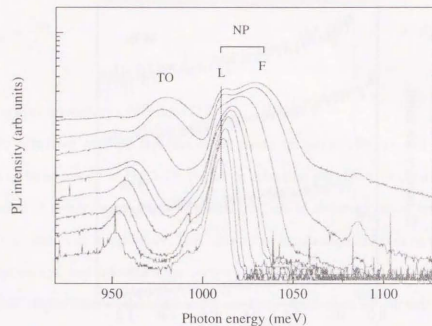


Fig.3-14 Typical excitation power dependence of PL spectra of NCS. With increasing excitation, relative NP intensity decreases and a new peak, F, appears.

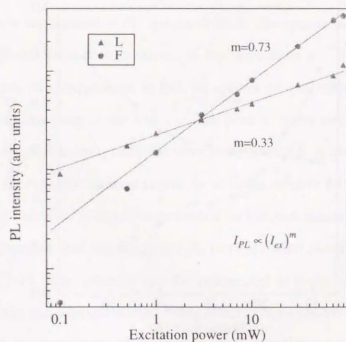


Fig.3-15 Excitation power dependence of integrated NP intensity of NCS. The NP peak was deconvoluted to two peaks, L and F. Strong saturation is seen in L compared to F.

These results of temperature and excitation power dependence and time-resolved PL support the idea that the enhanced NP feature comes from localized excitons in NCS. Possible candidates of localization center would be in-plane quantized energy variation due to the inhomogeneous strain and/or the interface roughness. The well width dependence of relative NP intensity would be helpful to find out which is the dominant factor for exciton localization since the former is supposed to be less sensitive to well width variation than the latter. The relative NP intensity of NCS at low excitation with fixed SiGe width of 10Å is plotted against Si well width in Fig.3-16 (a). Also, the first derivative of the quantized energy,

$$\frac{\partial E}{\partial L_{Si}} = \frac{\partial E_v}{\partial L_{Si}} + \frac{\partial E_h}{\partial L_{Si}} \quad (3.9)$$

is plotted as a function of the Si well width in Fig.3-16 (b). This parameter is proportional to the amount of in-plane energy variation if we assume that the roughness of the Si width exists and its amount is independent of the Si width. The correlation between these two is apparent and the strong well width dependence indicates that the interface roughness rather than the inhomogeneous strain is important to make localization centers. This idea was also supported by the well width dependence of the decay time of the NP line at 8K. The localization of the excitons is known to lead to elongation of the radiative lifetime due to the energy spreading in k-space [75], and resultant suppression of the coupling between excitons and photons. As clearly seen in Fig.3-17, the decay time was found to show a similar behavior with the well width dependence of the relative NP intensity, and show maximum at the Si width of =12Å.

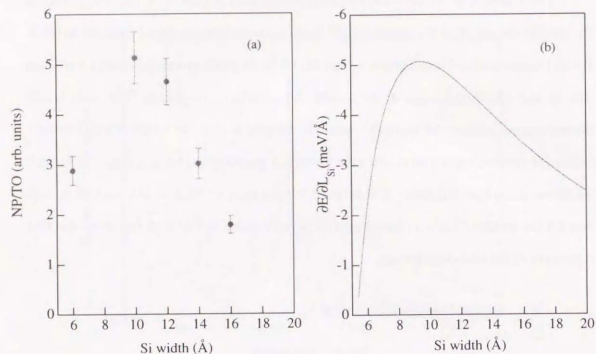


Fig.3-16 (a) The relative NP intensity measured with low excitation and (b) the calculated first derivative of the quantized energy of NCS with a fixed SiGe width of 10Å as a function of Si width.

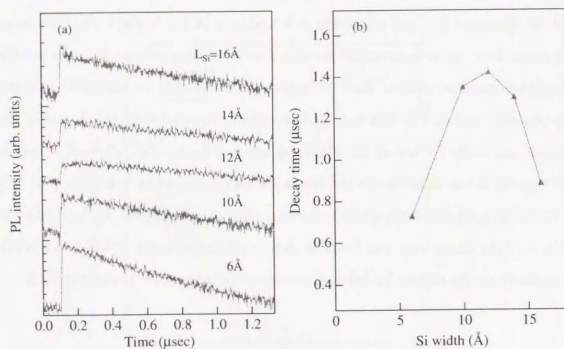


Fig.3-17 (a) Temporal profiles and (b) the decay time of the NP luminescence of NCS with a fixed SiGe width of 10Å as a function of Si width.

To further confirm that the interface roughness is the key to make localization centers for excitons, post-growth annealing has been performed. Post-growth annealing is considered to induce the atomic rearrangement, and resultant interface would be not abrupt but smooth compared to the original interface of the as-grown NCS. Figure 3-18 shows a comparison of NCS PL spectra of the as-grown sample and the samples annealed at 750 °C, and 850 °C for 20 minutes. Two series of spectra are shown with different Si widths of 10Å and 14Å. It is noted that the spectra were normalized to give the same TO intensity. In all the series of samples, as is expected, drastic quenching of NP intensity was found in the annealed-samples due to the reduction of the in-plane energy variation. The other change in PL spectra, the spectral blue-shift with increasing annealing temperature, is due to the potential distortion induced by the atomic interdiffusion [59]. Figure 3-19 compares excitation dependence of PL spectra of (a) as-grown and (b) annealed sample of Si width of 12Å. In the annealed sample, the peak position shifts to higher energies from at very low excitation region unlikely the as-grown sample. This indicates that the  $\delta$ -like density of states which would be the localization centers is removed by post-growth annealing. Therefore, the changeover from the saturation of the localization centers to the subsequent band filling, which can be clearly observed in the as-grown sample, is invisible in the annealed sample. This is also reflected in the weak dependence of the relative NP intensity on excitation power in the annealed sample.

Temperature dependence of the effective radiative lifetime is also greatly modified by post-growth annealing. Figure 3-20 shows temperature dependence of the effective radiative lifetime for as-grown and annealed NCS. It can be seen that the effective radiative lifetime of the annealed sample, especially the 850°C-annealed sample, depends on temperature and almost linearly increases with increasing temperature even at low temperatures unlikely the as-grown NCS. This suggests that the density of states in the annealed sample is not zero-dimensional but modified to two-dimensional.

Another way to modify the interface roughness is to perform the growth interruption at the centered interface during growth. For this purpose, a series of samples

were prepared with growth interruption at the strained-SiGe/strained-Si interface for 5 sec to 9 min. Figure 3-21 shows growth interrupted time dependence of PL spectra under low excitation power. It can be seen that the growth interruption was also found to modify the spectral feature of the NCS. With increasing growth interruption, relative NP intensity increases first. However, excess growth interruption was found to reduce relative NP intensity. It is found that the growth interruption time is also an important parameter to optimize the NP enhancement.

These results, the observed NP quenching and the modification of various optical properties support our idea that the exciton localization originating from in-plane energy variation due to the interface roughness brought the strongly enhanced NP feature observed in NCS. Finally, it should be pointed out that many efforts have been devoted to establish how to grow smooth and abrupt heterointerfaces, however, our study clearly showed that the existence of the interface roughness is very important to obtain enhanced NP luminescence. To develop a technology to control the interface roughness will be required for further improvement of the optical properties of the Si/SiGe system.

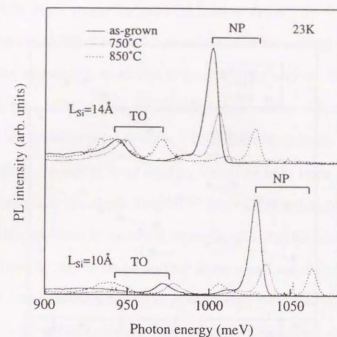


Fig.3-18 Comparison of PL spectra of the as-grown NCS and the annealed samples at 750 °C and 850 °C for 20 minutes. Selective reduction of NP intensity can be seen in the annealed samples.

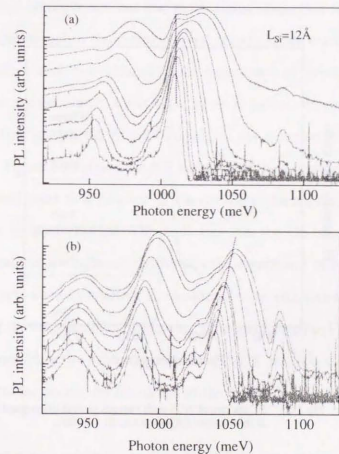


Fig.3-19 Excitation power dependence of PL spectra of (a) as-grown NCS and (b) annealed sample at 850 °C.

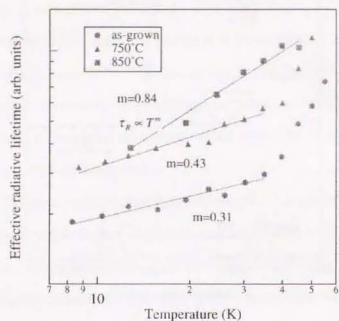


Fig.3-20 Temperature dependence of the effective radiative lifetime of NP lines of as-grown and annealed NCS.

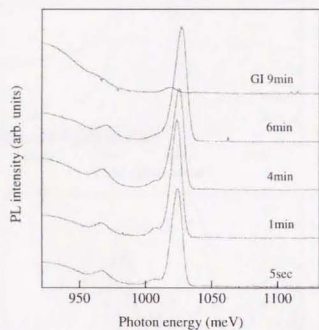


Fig.3-21 PL spectra of NCS with various growth interrupted time at the strained-SiGe/strained-Si interface.

### 3.5 NCS with pure-Ge/pure-Si active layer

The enhanced NP feature is quenched with increasing temperature due to the delocalization of excitons as shown in the previous section. In the case of NCS with  $10\text{\AA-Si}/10\text{\AA-Si}_{0.64}\text{Ge}_{0.36}$ , the critical temperature where delocalization takes place is  $\approx 40\text{K}$ . From the practical point of view, it is desirable to increase the critical temperature. For this purpose, "pure-Ge" was used as a confinement layer for holes. The pure-Ge layer would increase the depth (height) of the well (barrier) for holes (electrons) and strongly confine excitons in the active layer. In addition, the accumulated large strain in the Ge layer would lead to rough surface as an initial stage for the Stranski-Krastanov (SK) growth mode and the resultant *in-plane* energy variation would become large.

Figure 3-22 shows Ge width dependence of PL spectra of pure-Si/pure-Ge NCS. The enhanced NP feature was found with Ge width of 0.8 to 4.8 monolayers. The NP peak energy is plotted against Ge coverage in Fig.3-23. With increasing Ge width, the spectral red-shift is seen to saturate and an anomalous blue-shift takes place. This is due to the two-dimensional to three-dimensional growth mode changeover [16][76]. The formation of Ge islands is evidenced by the appearance of broad PL in the deep level. After emergence of Ge islands, a part of Ge atoms in the two-dimensional wetting layer is known to diffuse toward the islands, leading to the decrease of the thickness of the wetting layer. Figure 3-24 shows the full width at half maximum of the NP line from the two dimensional layer as a function of Ge coverage. An anomalous peak broadening occurs on the island formation. This indicates that the Ge island is initiated with a microscopic interface roughness, leading to the significant in-plane variation of the quantized energy. Such an interface is considered to be effective to increase the critical temperature of the delocalization of excitons. As demonstrated in Fig. 3-25, the enhanced NP feature was found to persist up to above 100K in  $10\text{\AA-Si}/3\text{ML-Ge}$  NCS. This directly reflects the successful formation of the deeper localization potential by using pure-Ge.

To demonstrate a possibility to apply NCS to the light-emitting diode, a preliminary experiment to achieve EL was performed. Nine pairs of the NCS were used for the active

layer, and the current was injected through Al Schottky contact. Figure 3-26 shows an EL spectrum obtained at 23K with injection current of 1mA. Luminescence from localized excitons in the NCS was clearly observed as evidenced by enhanced NP transition. Further optimization of the structure is, however, necessary for room temperature operation of light-emitting SiGe diode based on the NCS.

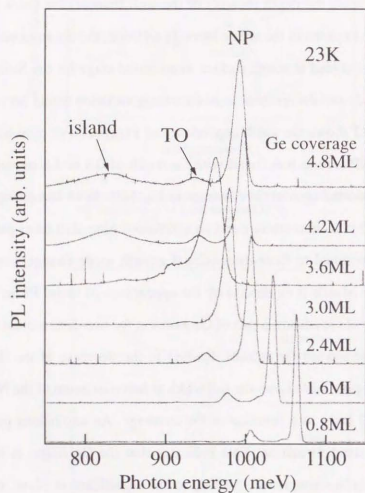


Fig.3-22 Ge coverage dependence of PL spectra of NCS with an active layer of 10Å-Si/pure-Ge.

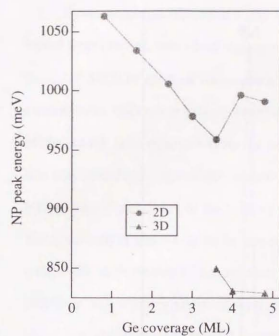


Fig.3-23 NP peak energy of pure-Si/pure-Ge NCS as a function of Ge coverage.

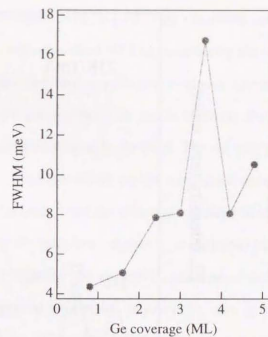


Fig.3-24 Full width at half maximum of NP peak as a function of Ge coverage.

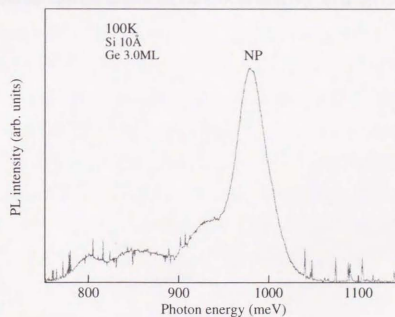


Fig.3-25 100K PL spectrum of 10Å-Si/3ML-Ge NCS. Note that NP line dominates the spectrum.

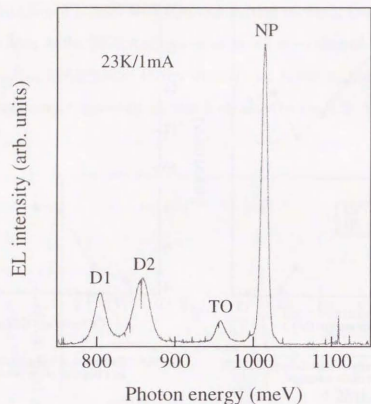


Fig.3-26 A typical EL spectrum of NCS at 23K with an injection current of 1mA.

### 3.6 Summary

Systematic spectroscopic study of Si-based NCS, a promising candidate for Si-based light emitter, was given. Intense PL with enhanced NP line was clearly observed from the NCS in spite of the indirect band structure in real- and k-spaces. Quantum confinement effect was clearly observed by varying the well width, showing that the enhanced NP lines originate from the expected transitions in the NCS. The enhanced NP line was found to be due to the exciton localization as evidenced by correlation between temperature dependence of the relative NP intensity and the effective radiative lifetime. The localization was likely to be caused by the interface roughness as indicated by the well width dependence of the relative NP intensity and selective reduction of the NP intensity and modification of various optical properties induced by post-growth annealing. An attempt to persist the enhanced NP feature was done by using a pair of pure-Si/pure-Ge as active layers, which is considered to construct deep localization potential through the interface roughness. Electroluminescence at low temperature was also demonstrated to show the potential of the NCS as a promising structure for the application to the light-emitting-diode.

## 4. SiGe/Si Quantum Wires on V-groove patterned substrates

### 4.1 Introduction

Artificially modulated semiconductor structures with reduced dimension such as quantum wires (QWRs) and dots (QDTs) are attracting great interest for the possibility of obtaining new and novel optical properties due to the quantum confinement effect [77]. Formation of high-quality heterointerfaces is essential for the observation of the quantum confinement effect. Combination of post-growth lithography and regrowth is one of the approaches which have been exploited. However, unintentional damage is likely to be induced during the process which degrades the optical properties by increasing nonradiative pathways. Hence, *in-situ* fabrication of QWRs taking advantage of the growth alone is more desirable since it is free from damage. Many efforts have been devoted to obtain such structures as QWRs and QDTs with high-quality which is an essential requirement to investigate their intrinsic optical properties. Invention of *in-situ* fabrication processes accelerated the progress in growing such low-dimensional semiconductor structures with high-quality. These processes include direct growth on patterned substrates [78]-[80], misoriented substrates [81], and cleaved edges [82]. In addition, utilization of selective epitaxial growth (SEG) [83]-[85] or self-organization [86]-[88] is also reported. One of the most successful results by utilizing these essentially damage free processes was reported by Kapon *et al* [78]. They fabricated QWR arrays on a V-groove patterned GaAs substrate by metal-organic chemical vapor deposition (MOCVD) where they clearly showed the existence of quantized states associated with QWRs at the bottom of the V-groove. They also demonstrated room temperature operation of a QWR laser on a V-groove patterned GaAs substrate [79]. As seen in these reports, there has been considerable progress in the *in-situ* fabrication of QWRs in GaAs/AlGaAs system. However, SiGe/Si QWRs which would stimulate much interest as a new semiconductor material has not been systematically studied.

In this chapter, a detailed study on fabrication and optical properties of SiGe/Si QWRs on V-groove patterned Si substrates is given. Section 4.2 describes the

experimental details, especially the process of QWR formation. Section 4.3 deals with CW PL and cathodoluminescence (CL) study. Three NP and TO pairs, which originate from the different spatial regions, were observed, and peak assignments were carried out. Section 4.4 is devoted to describe the results of time-resolved PL spectroscopy, which disclosed that the exciton diffusion induces the redistribution of photocarriers, and affects the optical properties. Section 4.5 introduces an attempt to use SEG to grow SiGe/Si QWRs only inside the V-groove. Optical anisotropy, which reflects the wire geometry, was found in EL from SiGe/QWRs at the bottom of the V-groove. A summary of this chapter is given in 4.6.

### 4.2 Fabrication of quantum wires

Figure 4-1 shows the process to fabricate V-groove patterned Si substrates. The starting material is a nominally on-axis p-type Si (001) wafer with resistivity of 5-10  $\Omega\text{cm}$ . On this wafer, a 1350Å  $\text{SiO}_2$  film which acts as a mask for chemical etching is formed by the thermal oxidation technique. In some cases,  $\text{Si}_3\text{N}_4$  films prepared by low pressure chemical vapor deposition (LPCVD) were alternatively used. Subsequently, by using a standard electron beam lithography technique, line-and-space patterns along the [110] direction with periods of 0.6-4.0  $\mu\text{m}$  are generated. Then, chemical etching with HF is performed to transfer the patterns to  $\text{SiO}_2$  film. After removing the resist, the substrate is dipped in  $\text{N}_2\text{H}_4$ -based solution or KOH-based solution in order to create a V-groove pattern with Si(111) facets. Figure 4-2 shows a cross sectional scanning electron microscope (SEM) image of a V-groove patterned Si substrate with a 0.6 $\mu\text{m}$  period. As shown in this figure, V-groove patterned Si substrates are reproducibly obtained by these lithography processes. Epitaxial growth was performed in a gas-source MBE system using disilane and germane as gaseous sources. Prior to growth, the substrate temperature was raised to 850  $^\circ\text{C}$  and held for 10 minutes in order to thermally desorb the contaminants and to obtain a clean surface. Then, the substrate temperature was lowered and the growth was commenced.

Figure 4-3 (a) shows the temperature dependence of the growth rate in gas-source MBE on planar Si (100) and Si (111) substrates with  $\text{Si}_2\text{H}_6$  flow rate of 2.5 sccm. Anisotropy of the growth rate (GR) on the different crystal orientations is found due to the difference of the decomposition kinetics of gaseous species. The anisotropy factor which is defined by  $\text{GR}_{(111)}/\text{GR}_{(100)}$  is plotted against the inverse of the growth temperature in Fig.4-3 (b). This factor increases with decreasing growth temperature, showing that low growth temperature is favorable for a successful realization of a sharp V-groove geometry which is effective to obtain small lateral dimension. However, it is known that the PL intensity strongly depends on the growth temperature environment [52][89], and a high temperature growth is favorable. As a candidate to satisfy these two conflicting claims, a thin Si buffer layer grown at high temperature would be effective. Hence, we performed the epitaxial growth at 740 °C with a thin Si buffer layer of less than 1000 Å. For the growth of the SiGe layer, the flow rate ratio of disilane and germane was kept as 1:1, which corresponds to Ge alloy composition of 0.18 on Si(100).

Figure 4-4 shows a typical TEM image of a SiGe/Si QWR grown on a V-groove patterned Si substrate. A very sharp V-form is seen as a thin dark band which represents the interface between the substrate and the Si buffer layer. The SiGe layer can be seen in a dark line along the [111] direction. At the bottom of the V-groove, an excellent crescent shape can be clearly seen in this micrograph. Any traces of misfit dislocations were not found. Since the growth time of the SiGe layer is 15 sec. in this sample, a vertical wire width of 85Å is expected from the simple estimation using nominal growth rate on Si(100) substrates. However, this micrograph shows that the vertical wire width is as thick as 150 Å. On the other hand, the well width of the quantum well fabricated on the Si(111) facets is much smaller than the expected value. Hence, the unexpectedly large value of the vertical wire width is accounted for by preferential mass transport from Si(111) towards the bottom of the V-groove due to the enhanced surface migration of adatoms on (111) compared to (100).

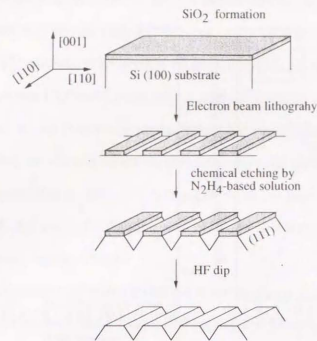


Fig.4-1 Fabrication process of V-groove patterned Si substrates.

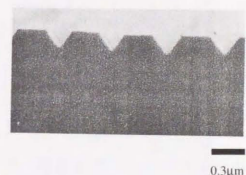


Fig.4-2 Cross-sectional SEM image of a V-groove patterned Si substrate with a 0.6μm period.

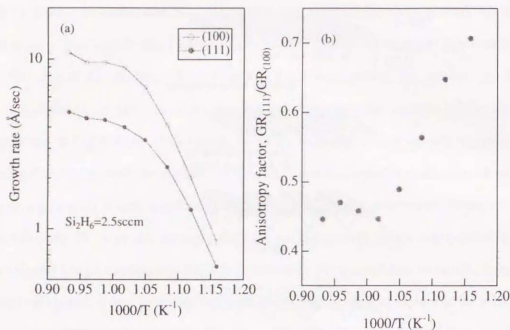


Fig.4-3 Temperature dependence of (a) growth rate of Si on Si (100) and Si (111) and (b) anisotropy factor of growth rate,  $GR_{(111)}/GR_{(100)}$ .

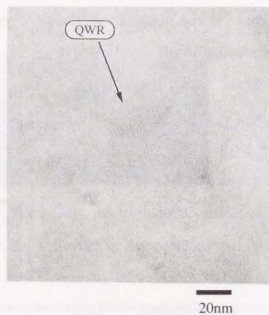


Fig.4-4 Typical cross-sectional TEM image of SiGe/Si on a V-groove patterned Si substrate.

### 4.3 Photoluminescence and Cathodoluminescence

Figure 4-5 shows 16K PL spectra of the SiGe/Si QWs grown on V-groove patterned Si substrates with periods of 2 $\mu$ m and 4 $\mu$ m. In addition to the PL from the Si substrate around 1097meV, many structures which overlap each other can be seen. These lines can be deconvoluted into three different NP and TO phonon replica pairs. The three pairs are likely to come from different regions since the samples can be divided into three different parts, that is, the (111) QWs, QWRs at the bottom of the V-groove, and the (100) QWs between the V-grooves. In order to carry out peak assignments, CL measurements were performed.

CL measurements were carried out at temperatures  $T \approx 5-70$ K using the CL mode of a SEM with electron beam energies between 10 and 15 keV and beam currents of 0.1nA. Custom-designed mirror optics were used to collect the luminescence and either direct a parallel beam into a Bruker IFS 66 Fourier transform spectrometer or focus the luminescence on a Ge photodetector. A narrow band pass filter was used to obtain a monochromatic image.

Figure 4-6 shows a CL spectrum recorded at  $T=5$ K from a sample with a 2 $\mu$ m V-groove period. Three distinct SiGe NP peaks and the corresponding TO replicas are observed. The feature is almost the same as the PL spectrum in Fig.4-5. Narrow band pass filters were selected centered at the three TO lines to obtain monochromatic CL images. Figure 4-7(a) shows the cross-sectional secondary electron images of a SiGe/Si QWR with a 4 $\mu$ m V-groove period. The monochromatic CL image obtained with a filter centered at TO<sub>1</sub> is shown in Fig.4-7(b). The distribution of the luminescence correlates with the positions of the SiGe(100) planar wells between the neighboring V-grooves. The broadened image with Gaussian broadening of  $\approx 1\mu$ m is believed to originate from the spatial diffusion of carriers. The distribution of (c) TO<sub>2</sub> has a triangular shape, while that of (d) TO<sub>3</sub> has a pronounced V-shape. From these images, it can be concluded that the three pairs originated from the (111) QWs, QWRs at the bottom of the V-groove, and the (100) QWs from the higher energy side, respectively.

The energy position of the (111) QWs is reasonable since it is in good agreement with the calculated results with a well width estimated by TEM ( $\approx 10\text{\AA}$ ). The energy of the (100) QWs is also reasonable since there is only a small deviation in energy between the (100) QWs on V-groove patterned substrates and on planar (100) substrates. However, the blue-shift of the QWRs compared to the (100) QWs cannot be intuitively understood. The lateral and vertical widths of the QWRs are  $\approx 300\text{\AA}$  and  $\approx 150\text{\AA}$ , respectively, which are too large to bring lateral quantization and the blue-shift. A possible candidate to explain the blue-shift is the built-in strain inside the V-groove. Since the SiGe layer inside the V-groove is surrounded by rigid Si, the strain would not be biaxial any more. As a rough estimation, we calculated Ge composition dependence of the bandgap of the cubic SiGe alloy with lattice constant of Si. Figure 4-8 compares excitonic indirect bandgap of unstrained and strained-SiGe with biaxial compressive and hydrostatic strains. It can be seen that the bandgap of the cubic SiGe alloy is larger than that of pseudomorphically strained-SiGe on Si. The bandgap of cubic  $\text{Si}_{0.82}\text{Ge}_{0.18}$  was found to be in good agreement with the NP PL energy of SiGe QWR. Therefore, the strain rather than the lateral confinement is likely to be a primary factor to bring the spectral blue-shift.

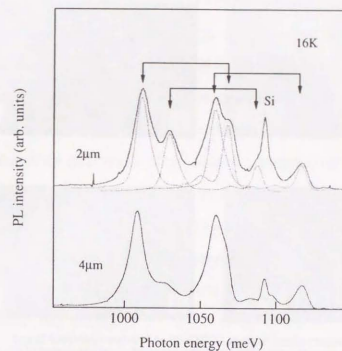


Fig.4-5 PL spectra of SiGe/Si QWs grown on V-groove patterned Si substrate with V-groove period of  $2\mu\text{m}$  and  $4\mu\text{m}$  at 16K.

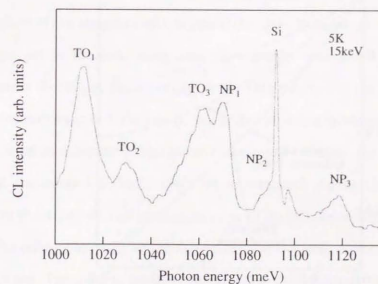


Fig.4-6 CL spectrum of SiGe/Si QWs grown on a V-groove patterned Si substrate with a  $2\mu\text{m}$  V-groove period at 5K.

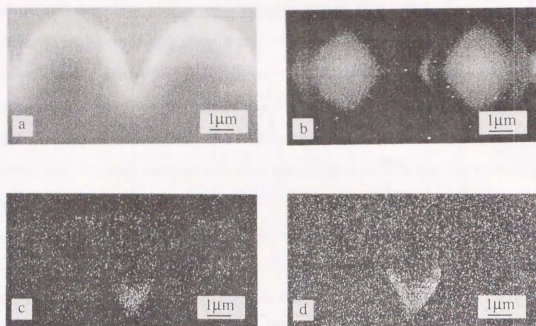


Fig.4-7 (a) Secondary electron image of SiGe/Si on V-groove patterned Si and (b)-(d) monochromatic CL images obtained with narrow bandpass filters.

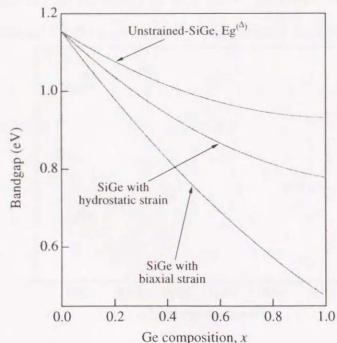


Fig.4-8 Calculated excitonic bandgap of cubic SiGe with lattice constant of Si (hydrostatic strain), pseudomorphically strained-SiGe on Si(100), and unstrained-SiGe.

#### 4.4 Exciton diffusion

As shown in the previous chapter, when one uses a V-groove patterned substrate for QWR fabrication at the bottom of the V-groove, two kinds of QWs are simultaneously formed on the (111) facet and the (100) flat region between the neighboring V-grooves reflecting the substrate geometry. Since the growth rate on the (111) facet is generally smaller than that on the (100) plane, the resultant quantized energy of the (111) QWs is larger than that of the other region. This could be a driving force of the exciton diffusion in the (111) QWs to the other regions, which is considered to strongly affect the optical properties of the system. Therefore, to understand the dynamics of the exciton diffusion in the (111) QWs is quite essential for device design using V-groove patterned substrates. Particularly, in the case that the lifetime of the carrier is long like SiGe/Si QWs [90], this problem becomes very critical.

Figure 4-9 shows PL spectra of the 2 $\mu$ m-period sample at 16K and 31K. It can be seen that the relative intensity of three peaks dramatically changes with temperatures. At 31K, the PL spectrum is dominated by the emission from the (100) QWs and the emissions from the other two regions are hardly identified. Systematic temperature variation clarified that the emission from the (100) QWs becomes stronger with increasing temperature, while the total integrated PL intensity was found to be temperature independent at T<40K as shown in Fig. 4-10. This means that the participation of the nonradiative pathways in SiGe can be negligible in this temperature range since their thermal activation at higher temperatures is supposed to reduce the total intensity. It is noted that the control SiGe/Si QWs on unpatterned region showed temperature independent PL at T<40K, and such an increase of the PL intensity of (100) QWs cannot be seen. The relative intensity of the three pairs also depends on the V-groove period as seen in Fig.4-5. The relative intensity of the (111) QWs compared to other regions is stronger in the 4 $\mu$ m-period sample than in the 2 $\mu$ m-period sample. It is remarked that the peak positions of these three pairs well coincide, indicating that no significant well width variation exists between these two samples. In addition, it should be stressed that these samples were simultaneously grown. Therefore, it would be possible to assume that these

two samples have the same radiative and nonradiative lifetimes. These results indicate that significant carrier redistribution takes place before photogenerated carriers radiatively recombine.

The exciton diffusion seems to play an important role to account for these results. The captured excitons in the SiGe layer would tend to diffuse to the lower energy region within their lifetime. For our samples, the lowest energy region is the (100) QWs. Therefore, the observed temperature variation of the PL intensity can be explained by assuming that the diffusivity is an increasing function of the temperature, which would give a longer length for the excitons to diffuse to the (100) QWs. The V-groove period variation can be also explained in the same context. The shorter the V-groove period is, the more excitons can diffuse to the (100) QWs within their lifetime. In order to confirm this idea, time-resolved PL measurements were performed.

Figure 4-11 shows the V-groove period dependence of the temporal PL profile of the (111) QWs at 16K. The faster decay time is observed when the V-groove period decreases, suggesting that the exciton diffusion plays an important role. The PL intensity is proportional to the number of excitons in the (111) QWs if the radiative lifetime is constant. As already discussed, this assumption is plausible in this case since these three samples were grown simultaneously and have no well width variation which lead the same radiative lifetime. Therefore, the observed faster decay time of the shorter-period sample can be attributed to the reduction of the number of the exciton inside the (111) QWs due to the diffusion to the other regions. That is, the decay time is determined by the competition between radiative recombination and the exciton diffusion.

Figure 4-12 shows the temperature dependence of the decay time for the (111) QWs and the (100) QWs with V-groove period of a 2 $\mu$ m. The decay time of the (100) QWs is found to be an increasing function of temperature in the lower temperature region. The decrease at higher temperatures would be participation of the nonradiative pathways. The behavior in the lower temperature region is a normal behavior for two-dimensional excitons if we consider that the exciton with center-of-mass wave vector  $k < k_0$  can decay radiatively [72]. By using Maxwell-Boltzman distribution and two-dimensional density of

states, the following expression can be obtained for the averaged lifetime  $\tau(T)$  in the lower temperature region [73]

$$\tau(T) \propto \tau_0 \frac{k_0 T}{\Delta} \quad (4.1)$$

where  $\tau_0$  is the intrinsic lifetime of the exciton at  $k = 0$ , and  $\Delta$  is the maximum kinetic energy of excitons which can decay radiatively. Although the radiative decay time of the (111) QW exciton is also thought to be an increasing function of temperature, the observed decay time shows an anomalous behavior and decreases with increasing temperature. This result can also be explained by the exciton diffusion. The concentration  $n(x)$  of excitons in the (111) QWs is obtained by calculating the following diffusion equation:

$$\frac{\partial n}{\partial t} = D \frac{\partial^2 n}{\partial x^2} - \frac{n}{\tau} \quad (4.2)$$

where  $D$  is the diffusivity of excitons. By assuming that the PL intensity of the (111) QWs is proportional to the integration of  $n(x)$  in this region, it was found that the temporal PL profile is well reproduced and the diffusion length  $\sqrt{D\tau}$  can be obtained. This method is analogous to that of Hillmer and his co-workers who used a microstructured mask for time-resolved PL and investigated lateral motion of two-dimensional excitons in GaAs/AlGaAs QWs [91]. When fitting the temporal profiles, we assumed that the radiative lifetime of the (111) QWs has the same temperature dependence as the (100) QWs. This assumption leaves us ambiguity in the determination of the absolute value of the diffusivity. Therefore, we mention here only the diffusion length. Separate measurements of the radiative lifetime of (111) QWs are required to make the diffusivity only fitting parameter for reproducing the temporal profiles.

Figure 4-13 shows the temperature dependence of the diffusion length. It is seen that the diffusion length increases with increasing temperature. This means that more excitons captured into the (111) QWs can diffuse to the other regions before radiative recombination at higher temperatures. By utilizing this characteristics, it would be possible to concentrate carriers to one small region, preferably to the QWR region, which is useful for device applications.

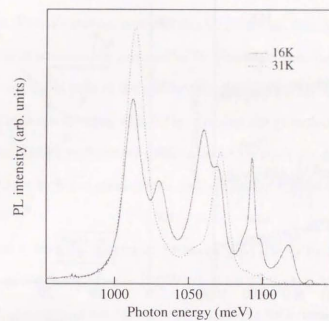


Fig 4-9 PL spectra of the 2 $\mu$ m-period sample at 16K and 31K.

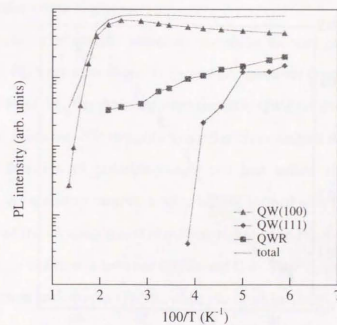


Fig.4-10 Temperature dependence of integrated PL intensity of different three regions, (100)QW, (111)QW, and QWR.

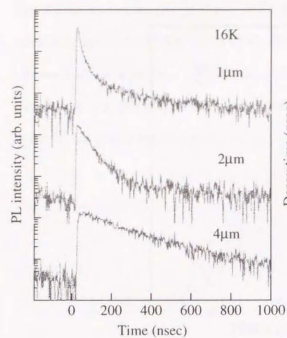


Fig.4-11 V-groove period dependence of temporal profiles of NP emission of the (111) QWs.

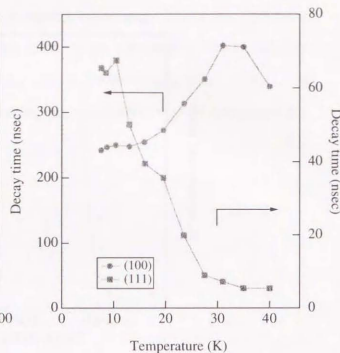


Fig.4-12 Temperature dependence of decay time of NP emission of (100) and (111) QWs.

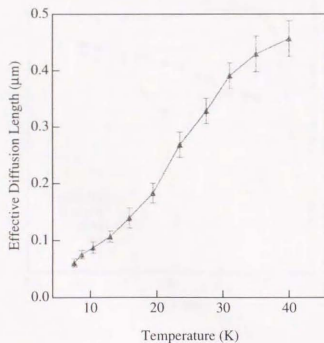


Fig.4-13 Temperature dependence of the effective diffusion length of excitons in (111) QWs deduced by reproducing temporal profiles.

#### 4.5 Selective epitaxial growth of quantum wires

The study in the previous chapter clarified the possibility to concentrate excitons to the QWR region. Two alternative methods can be proposed. One is to reduce the area of the (100) flat region between the grooves of the patterned substrate and to fabricate the QWR at the top and the bottom of the groove. The other is to exploit SEG technique, that is, the (100) flat region is covered with SiO<sub>2</sub> to realize the growth only inside the groove. The latter can be readily realized by gas-source MBE since no dangling bonds can be available on SiO<sub>2</sub> which are prerequisite for adsorption of decomposed source gases [92][93].

Figure 4-14 shows PL spectra of Si/Si<sub>0.82</sub>Ge<sub>0.18</sub>/Si QWs grown on a planar Si (100) substrate as a control sample (SQW), and by SEG on a V-groove patterned Si substrate. The thicknesses of the Si buffer layer and the SiGe well are nominally 240Å, and 34Å for a planar Si substrate, respectively. In the both spectra, we can clearly see a pair of peaks which can be identified as NP and TO replica. The spectral blue-shift due to the strain can be clearly observed, suggesting the pair comes from the wire-shape SiGe formed at the bottom of the V-groove.

In order to clarify the specific properties brought by the wire geometry, polarization measurements in EL were carried out. A typical EL spectrum from the SiGe QWRs at 18K is shown in Fig.4-15. The emission from the SiGe QWRs is dominant compared to that from the Si substrate. NP intensity from the cross section and the surface was measured as a function of polarizer angle put just before the entrance of the monochromator. As a control sample, a SiGe/Si QW formed on a planar substrate was used. The result of the cross-sectional emissions is shown in Fig.4-16. It is remarkable that the polarization is different between QWRs and QW. That is, no polarization is seen in the cross-sectional emission in QWRs, while the cross sectional EL from the control SiGe/Si QW shows a strong in plane, i.e., transverse electric (TE) polarization. On the other hand, NP emission from the surface showed a strong anisotropy in EL, polarization of 24% in the [110] direction (parallel to the wire). This is also in contrast to the surface normal EL of the control QW which gives rise to no preferential polarization in the QW

plane. These results clearly show the realization of luminescent SiGe layers with wire geometry.

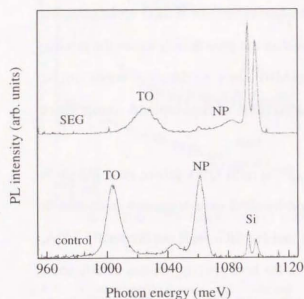


Fig.4-14 Comparison of PL spectra of SiGe/Si QWRs grown on planar (100) and V-grooved substrates.

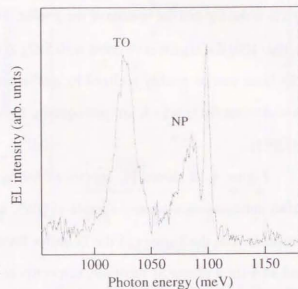


Fig.4-15 Typical EL spectrum of SiGe/Si QWRs grown by SEG.

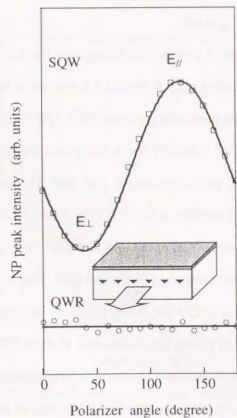


Fig.4-16 Polarization dependence of NP intensity of cross-sectional emission of QWRs and control QWRs.

#### 4.6 Summary

The SiGe/Si QWR arrays on V-groove patterned Si substrates have been grown by gas-source MBE. Crescent shaped SiGe layer was evidenced by TEM cross sectional imaging. Three NP and TO pairs were observed, and they were identified as coming from the (111) QW, the QWR, the (100) QW from the higher energy side, respectively. Inhomogeneous strain inside the V-groove was found to give significant effect on the energy of the SiGe QWR.

Dynamics of exciton diffusion was investigated by using time-resolved photoluminescence spectroscopy. The decay time of the luminescence from the (111) facet QWs was found to be strongly dependent on the V-groove period and to decrease with the V-groove period. Temperature variation clarified that the increase of temperature leads to the reduction of the decay time of the (111) QWs in contrast to the radiative lifetime of two-dimensional excitons. These behaviors were explained in terms of the competition between radiative recombination and the exciton diffusion to the other regions, that is, the (100) QWs and the QWRs at the bottom of the groove. Diffusion length of the excitons in the (111) QWs was determined from the temporal profile of the luminescence.

Selective epitaxial growth was attempted to fabricate QWRs which can efficiently collect excitons inside the V-groove. The PL spectrum was dominated by the emission from the QWR. The wire-specific optical anisotropy was found in the electroluminescence.

## 5 Strain-induced quantum nanostructure

### 5.1 Introduction

Heteroepitaxial growth of highly lattice-mismatched materials such as InGaAs/GaAs [86]-[88], and Ge/Si [16][76], has been gaining increasing interests since it offers the possibility to fabricate semiconductor quantum dots (QDTs) via Stranski-Krastanov (SK) growth mode without any processing. Under appropriate growth conditions, the formation of highly ordered island arrays with high density was observed. The application of the  $\delta$ -like density of states of QDTs to the semiconductor lasers is expected to bring very low threshold current and high  $T_0$  [94]. In fact, the zero-dimensional feature of InGaAs dots has been evidenced by ultranarrow luminescence from a single QDT [95][96] and micro photoluminescence excitation spectroscopy [97] which can probe the density of states of single QDTs. Device applications of the QDTs formed by the SK mode have been also intensively studied, including vertical surface light emitting laser diode with active layer of InAs QDTs [98], novel FETs with InAs QDTs as confinement layer for electrons [99], and so on. As illustrated by these demonstrations, the SK mode is quite promising as a method to fabricate QDTs.

The "stressor", which induces strain-field to buried layers, is known to be useful to fabricate low-dimensional semiconductors. The stressor locally modulates the potential of the buried layers through the lattice deformation. In fact, strain-induced QWRs are demonstrated by fabricating Cr [100] or InGaAs [101] gratings as stressors with conventional lithography processes. However, the lateral dimension is limited by the spatial resolution of the lithography techniques. To overcome this problem, the islands formed by the SK mode would be effective. Since the SK growth mode proceeds with a partial strain relaxation in the islands, the islands are probable to generate strain-field and act as stressors.

In this chapter, we show that Ge islands formed by the SK mode act as stressors to induce inhomogeneous strain to the buried layers and bring significant bandgap modulation. In addition, a novel technique to control the position and the size of

semiconductor islands is proposed. The method is to perform overgrowth on a cleaved edge of strained multiple quantum wells (SMQWs) which acts as a substrate with *in-plane* modulated lattice constant and gives periodically modulated strain to the epitaxial layer. Its successful application is demonstrated by using Ge islands.

### 5.2 Lateral band gap modulation by Ge island stressor

The samples are 34Å-Si<sub>0.82</sub>Ge<sub>0.18</sub>/Si QWs with surface Si<sub>1-x</sub>Ge<sub>x</sub> islands. Figure 5-1 shows AFM image of Si<sub>0.36</sub>Ge<sub>0.64</sub> island grown at 700 °C. As shown in this figure, the SiGe layer is corrugated in a self-organized manner with period of  $\approx 1000\text{Å}$ , and height of  $\approx 100\text{Å}$ . Driving force of this self-organization is minimization of surface free energy including strain contribution. It is difficult to quantitatively estimate the strain component inside the SiGe 3D island. However, as a consequence of 3D growth, a part of strain inside the SiGe 3D island is released and non-diagonal term of strain component is supposed to exist.

To investigate whether the 3D island acts as a stressor to the buried SiGe/Si QWs or not, PL spectroscopy was performed. Figure 5-2 shows 16K PL spectra of Si<sub>0.82</sub>Ge<sub>0.18</sub>/Si QWs with Si<sub>1-x</sub>Ge<sub>x</sub> 3D island on the surface. Ge composition in the 3D island,  $x$ , was chosen as nominally 0.81. A striking feature is that PL energy shifts to lower energies with decreasing Si spacer thickness. The amount of the energy shift increases with increasing Ge composition in the 3D island. It is remarked that no coupling of electronic states between the surface SiGe islands and the SiGe QWs is expected for the Si spacer thickness above 100Å. Also, the surface electric field cannot be responsible for this energy shift. This is excluded since we independently grew Si<sub>0.82</sub>Ge<sub>0.18</sub>/Si QWs with different overlayer thickness, and checked that no energy shift is observed. Therefore, undoubtedly, we can conclude that the SiGe 3D island induced strain field to buried Si<sub>0.82</sub>Ge<sub>0.18</sub>/Si QWs and caused PL peak energy shift.

Figure 5-3 shows (a) NP peak energy and (b) full width at half maximum (FWHM) as a function of the Si spacer thickness. With increasing (decreasing) strain (Si spacer thickness), NP peak shifts to lower energies and FWHM shows broadening reflecting the

island size distribution. In order to estimate the amount of strain, a preliminary calculation was performed by assuming that the SiGe/Si QWs are pseudomorphically grown on a substrate with larger lattice constant than Si. The largest energy shift of 23meV in the 500Å-spacer sample was found to correspond to  $\approx 0.18\%$  increase of in-plane lattice constant. With increasing Si spacer thickness from 500Å, the amount of the strain was found to decrease with decay length of a few thousand Å. This shows that 2D growth breakdown causes lattice distortion as deep as a few thousand Å and possibly induces significant change in optical and transport properties of the underlying materials, which should be carefully taken into account in device design using self-organized semiconductor islands.



Fig.5-1 AFM image of SiGe islands grown at 700 °C.

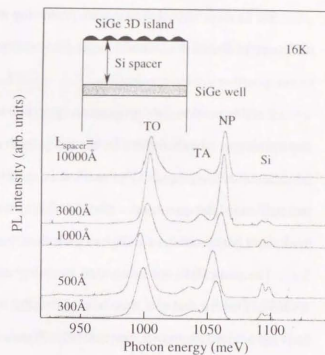


Fig.5-2 Si spacer thickness dependence of PL spectra of SiGe/Si QWs with islands.

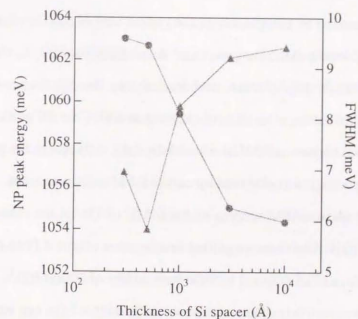


Fig.5-3 NP peak energy and FWHM as a function of Si spacer layer thickness.

### 5.3 Control of Ge island formation by cleaved edge overgrowth

SK mode is regarded as a quite promising method to fabricate QDTs. However, it is necessary to establish a method to precisely control the size and the position of the islands before possible device applications.

For this purpose, we propose an approach to control the position and the size of the semiconductor islands formed by the SK growth mode, and demonstrate its application to fabrication of Ge islands. The method is to perform overgrowth on a cleaved edge of strained multiple quantum wells (SMQWs) which acts as a substrate with *in-plane* modulated lattice constant and gives periodically modulated strain to the epitaxial layer.

The samples were fabricated by using solid-source MBE system (VG-Semicon V80M). The Si and Ge flux was provided by an electron-beam evaporator and a conventional effusion cell, respectively. Figure 5-4 illustrates (a) the growth process of our method and (b) the  $\text{Si}_{0.8}\text{Ge}_{0.2}/\text{Si}$  SMQW which were used as substrates for the cleaved edge overgrowth. The SMQW consists of a series of 5-period  $\text{Si}_{0.8}\text{Ge}_{0.2}/\text{Si}$  SMQW with different SiGe widths of 200 to 400 Å and fixed Si width of 300 Å. Each SMQW is separated by a 1000 Å Si spacer layer. It is noted that the width of the  $\text{Si}_{0.8}\text{Ge}_{0.2}$  is chosen to be comparable to the typical size of the Ge islands (200-750 Å) formed in the SK mode. After the growth of the SMQWs at 500 °C, the substrate was cleaved, dipped in an HF solution, and loaded into the MBE chamber again. The overgrowth was carried out after thermal cleaning at 800 °C for 20 minutes. The amount of the Ge layer was chosen as 6 ML to exceed the critical thickness for island formation. The surface morphology was observed by *ex-situ* AFM in tapping mode.

Figure 5-5 shows AFM images of the 6 ML of Ge on the cleaved edge of the  $\text{Si}_{0.8}\text{Ge}_{0.2}/\text{Si}$  SMQW. The three magnified images were obtained from different parts of the same substrate, and correspond to SiGe well widths of 200 Å, 300 Å, and 400 Å from the upper side, respectively. Three-dimensional growth of Ge can be seen in all the images, as is expected. Importantly, the arrangement of the Ge islands is not random but shows regularity reflecting the substrate geometry. In addition, the height of the islands is seen to become larger as the SiGe well width of the SMQW is increased. From the cross-

sectional profile perpendicular to the SMQW (growth direction of the first growth), it was found that the number of the peaks agrees with the number of Si spacer layers. Therefore, it can be concluded that the Ge islands were selectively formed on the Si layers. The reason for this selectivity will be discussed later.

To carry out a quantitative evaluation, two-dimensional fast Fourier transform (FFT) was carried out. Figure 5-6 shows typical results of FFT, which were carried out on Ge on 300 Å-Si/400 Å-SiGe, along different two directions; (a) perpendicular and (b) parallel to the first growth as shown by the arrows. Both curves are dominated by one Fourier component with selected frequency, indicating that the island formation took place periodically. The size of the island, defined as the main peak of the FFT curve, is plotted for different two directions (a) and (b) as a function of the SiGe width of the SMQW in Fig. 5-7. Since the Ge islands are grown on the Si, the size perpendicular to the first growth is supposed to coincide with the Si width of 300 Å. However, it was found that the island size linearly increases with increasing SiGe width as shown in Fig. 5-7 (a), indicating that Ge adatoms on SiGe diffuses toward the Ge islands once the Ge islands are formed on Si. In other words, the size of the islands can be controlled by the well width of the SMQW, which in turn can be precisely controlled by the first MBE growth.

In order to check if the preferential site for island formation depends on growth temperature, another overgrowth was performed at 600 °C. Figure 5-8 (a) shows an AFM image of the 6 ML of Ge on the cleaved edge of the  $\text{Si}_{0.8}\text{Ge}_{0.2}/\text{Si}$  SMQW grown at 600 °C. It can be readily seen that the density of the Ge islands is small on the cleaved edge of the Si cap and buffer layers. On the other hand, dense island formation can be observed on the cleaved edge of the SMQW. To clarify the preferential site of the island formation, the squared part of Fig. 5-8 (a) was magnified and the averaged cross sectional profile was calculated for the direction perpendicular to the first growth (A-B) as shown in Fig. 5-8 (b). In contrast to the case of 500 °C growth, the number of the peak in the SMQW coincides with not that of the 300 Å-Si spacer layers, 4, but that of the SiGe wells, 5. In addition, Ge islands can be hardly identified on the 1000 Å-Si spacer layer (the region inside the dotted lines) as shown in Fig. 5-8 (b). Therefore, it can be concluded that the

preferential site for the island formation is dependent on growth temperature, and Ge islands were selectively formed on the SiGe wells at 600 °C.

The dependence of the preferential site on temperature can be explained in terms of the balance of energetics and kinetics as follows. In view of energetics, SiGe of the SMQW is considered to be a more favorable site for overgrown Ge atoms since the smaller lattice-mismatch reduces the accumulated strain energy. Therefore, if the growth condition is nearly in thermoequilibrium, that is, high growth temperature and/or low growth rate, Ge adatoms would selectively be grown on SiGe since they could find energetically stable SiGe sites. After a few ML of growth, the Ge growth mode would transform from two-dimensional to three-dimensional. This explains why Ge islands are formed on SiGe at 600 °C. This idea is also supported by recent observations of the vertically aligned islands, where they are formed on top of the buried islands due to the surface strain field when the thickness of the spacer layer is thin [102]-[104]. On the other hand, when the growth temperature is 500 °C, the surface migration length of Ge atoms would be smaller due to kinetic suppression at lower temperatures. Therefore, some of the Ge atoms are considered to be grown on the Si. Since the critical thickness for the island formation on Si is smaller than that on SiGe, nucleation for island formation would occur on Si. Once Ge islands are formed on Si, the energetically favorable sites for Ge change from SiGe to Si and selective island formation takes place on Si.

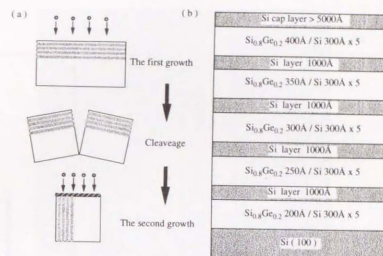


Fig.5-4 Schematic of (a) growth process and (b) structure of the SiGe/Si SMQW, which were used as substrates for cleaved-edge overgrowth.

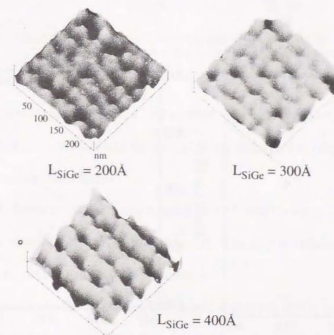


Fig.5-5 AFM images of 6ML of Ge on the cleaved edge of the SiGe/Si SMQW grown at 500 °C.

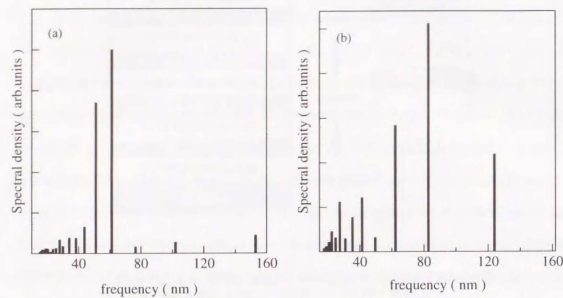


Fig-5-6 Typical results of FFT, which were carried out on AFM images of 6ML Ge on 300Å-Si/400Å-SiGe along (a) perpendicular and (b) parallel to the first growth direction.

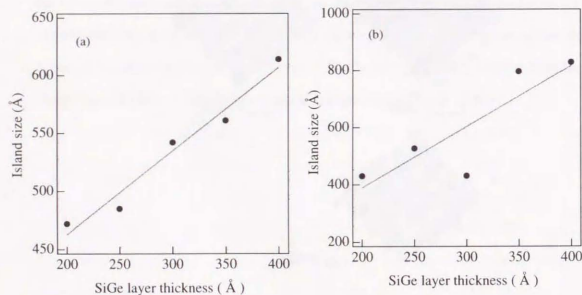


Fig-5-7 The size of the Ge islands defined as a main peak of FFT as a function of the SiGe width of the SMQW for different two directions (a) perpendicular and (b) parallel to the first growth.

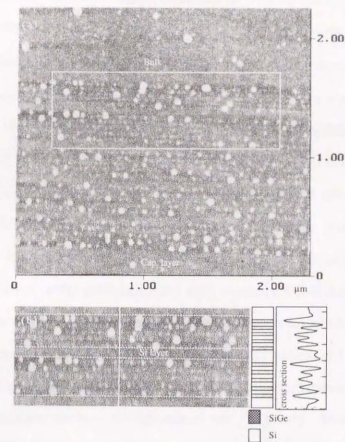


Fig-5-8 AFM images of 6-ML Ge islands on the cleaved edge of SiGe/Si SMQW grown at 600 °C (a) with low magnification and (b) the squared region in (a).

#### 5.4 Summary

Low-dimensional structures fabricated by heteroepitaxy of highly lattice-mismatched materials, which can be possible candidates for improvements of optical properties, are briefly introduced.

Ge islands formed by SK growth mode were found to act as stressors which induce inhomogeneous strain field to the buried layers. The strain-induced modification of the band structure would be useful to obtain islands.

Cleaved edge overgrowth on strained multiple quantum wells is used as a method to control the size and the position of the semiconductor islands formed by SK mode. By growing 6ML Ge on the cleaved edge of the strained SiGe/Si QWs at 500 °C, Ge islands were selectively formed on the Si layer and the size was controlled by the SiGe width. At 600 °C, the preferential site changed to the SiGe layer driven by the smaller lattice mismatch.

## 6 Conclusions

Various heterostructures based on SiGe/Si were proposed and fabricated by MBE. The structures were purposely designed to improve the luminescence efficiency by utilizing the flexibility of band engineering owing to the strain.

NCS, which has been proposed to improve the luminescence efficiency of indirect semiconductors, was applied to SiGe/Si heterostructures. Drastic enhancement of the luminescence, especially the NP luminescence, was observed in NCS compared to not only type-II strained-Si QWs but also type-I strained-SiGe QWs. Systematic well width variation evidenced that the observed luminescence is radiative recombination of excitons confined in NCS. The origin of the NP enhancement was found to be exciton localization due to the in-plane energy variation owing to the interface roughness. By replacing the QWs for holes with "pure-Ge", the enhanced NP feature persisted up to higher temperatures. Further optimization of the structure would bring room-temperature emission with the enhanced NP feature.

The SiGe/Si QWR arrays on V-groove patterned Si substrates were grown by gas-source MBE. Non-biaxial strain inside the V-groove resulted in the increase of the bandgap of the QWR at the bottom of the V-groove. Time-resolved PL study clarified that the distribution of photogenerated carriers is greatly affected by competition of exciton diffusion and radiative recombination. The diffusion length in the facet QW was found to be an increasing function of temperature, indicating that it is possible to concentrate carriers in a specific region at high temperatures. By exploiting selective epitaxial technique, PL spectrum was dominated by emissions from QWRs. The wire-specific optical anisotropy was found in the electroluminescence.

Other candidates for optical applications, strain-induced QDTs and self-organized QDTs, were briefly introduced. A method to control the size and the position of QDTs was proposed and applied to Ge islands.

As shown by these studies, SiGe/Si heterostructures are promising materials for possible optical device applications. Hopefully, this work will accelerate the study of Si-based heterostructures as photonic materials and contribute to the realization of the marriage with the advanced Si technology.

## References

- 1 For a review: R. A. Soref, Proc. of the IEEE **81**, 1685 (1993).
- 2 "Properties of strained and relaxed Silicon Germanium", edited by E. Kasper, INSPEC, the Institution of Electrical Engineers, London, United Kingdom (1995).
- 3 F. Scaffler, D. Többen, H. J. Herzog, G. Abstreiter, and B. Hollander, Semicon. Sci. Technol. **7**, 260 (1992).
- 4 Y. H. Xie, F. A. Fitzgerald, D. Monroe, P. J. Shilverman, and G. P. Watson, J. Appl. Phys. **73**, 8364 (1993).
- 5 K. Ismail, M. Arafa, K. L. Saenger, J. O. Chu, and B. S. Meyerson, Appl. Phys. Lett. **66**, 1077 (1995).
- 6 A. Yutani, and Y. Shiraki, Semicon. Sci. Technol. **11**, 1009 (1996).
- 7 A. Gold, Phys. Rev. **B35**, 723 (1987).
- 8 P. J. Wang, B. S. Meyerson, F. F. Fang, J. Nocera, and B. Paker, Appl. Phys. Lett. **55**, 2333 (1989).
- 9 T. E. Whall, D. W. Smith, A. D. Plews, R. A. Kuibak, P. J. Phillips, and E. H. C. Parker, Semicon. Sci. Technol. **8**, 615 (1993).
- 10 E. Kasper, H. Kibbel, H. J. Herzog, and A. Gruhle, Jpn. J. Appl. Phys. **33**, 2415 (1994).
- 11 R. P. G. Karunasiri, J. S. Park, Y. J. Mii, and K. L. Wang, Appl. Phys. Lett. **57**, 2585 (1990).
- 12 T. Fromherz, E. Koppensteiner, M. Helm, G. Bauer, J. F. Nützel, and G. Abstreiter, Phys. Rev. **B50**, 15073 (1994).
- 13 K. Fujita, S. Fukatsu, Y. Shiraki, H. Yaguchi, and R. Ito, Appl. Phys. Lett. **61**, 210 (1992).
- 14 J. S. Park, R. P. G. Karunasiri, and K. L. Wang, Appl. Phys. Lett. **61**, 681 (1992).
- 15 H. Sunamura, S. Fukatsu and Y. Shiraki, J. Cryst. Growth **150**, 1038 (1995).
- 16 H. Sunamura, N. Usami, Y. Shiraki, and S. Fukatsu, Appl. Phys. Lett. **66**, 3024-3026 (1995).
- 17 Q. Mi, X. Xiao, J. C. Sturm, L. C. Lenchyshyn, and M. L. W. Thewalt, Appl. Phys. Lett. **60**, 3177 (1992).
- 18 S. Fukatsu, N. Usami, Y. Shiraki, A. Nishida, and K. Nakagawa, Appl. Phys. Lett. **63**, 967 (1993).
- 19 H. Hasegawa, Phys. Rev. **129**, 1029 (1963).
- 20 C. Hering, and E. Vogt, Phys. Rev. **101**, 944 (1956).
- 21 R. Braunstein, A. R. Moor, and F. Herman, Phys. Rev. **109**, 695 (1958).
- 22 J. Weber, and M. I. Alonso, Phys. Rev. **B40**, 5683 (1989).
- 23 D. J. Robbins, L. T. Canham, S. J. Barnett, A. D. Pitt, and P. Calcott, J. Appl. Phys. **71**, 1407 (1992).
- 24 C. G. Van de Walle, and R. M. Martin, Phys. Rev. **B34**, 5621 (1986).
- 25 K. Nakura et al. Appl. Phys. Lett. **60**, 195 (1992).
- 26 P. A. M. Rodrigues, F. Cerdeira, and J. C. Bean, Phys. Rev. **B46**, 15263 (1992).
- 27 J. F. Morar, P.E. Batson, and J. Tersoff, Phys. Rev. **B47**, 4107 (1993).
- 28 H. Hirayama, T. Tatsumi, and N. Aizaki, Appl. Phys. Lett., **52**, 1484 (1987).
- 29 S. M. Gates, and S. K. Kulkarni, Appl. Phys. Lett. **60**, 53 (1992).
- 30 Y. Yasuda, Y. Koide, A. Furukawa, N. Ohshima, and S. Zaima, J. Appl. Phys. **73**, 2288 (1993).
- 31 K. Eberl, G. Krotz, R. Zachai, and G. Abstreiter, J. Phys. Collq. C (Paris) **5**, 329 (1987).
- 32 S. S. Iyer, J. C. Tsang, M. W. Copel, P. R. Pukite, and R. M. Tromp, Appl. Phys. Lett., **54**, 219 (1989).
- 33 P. C. Zalm, G. F. A. van de Walle, D. J. Gravesteijn, and A. A. van Gorkum, Appl. Phys. Lett., **55**, 2520, (1989).
- 34 K. Fujita, S. Fukatsu, H. Yaguchi, T. Igarashi, Y. Shiraki, and R. Ito, Jpn. J. Appl. Phys. **29**, L1981 (1990).
- 35 S. Fukatsu, K. Fujita, H. Yaguchi, Y. Shiraki, and R. Ito, Mat. Res. Soc. Symp. Proc. **220**, 217 (1990).
- 36 S. Fukatsu, K. Fujita, H. Yaguchi, Y. Shiraki, and R. Ito, Appl. Phys. Lett. **59**, 2103 (1991).
- 37 S. Fukatsu, K. Fujita, H. Yaguchi, Y. Shiraki, and R. Ito, Surf. Sci., **267**, 79 (1992).
- 38 J. Harris, D. Ashenford, C. Foxen, P. Dobson, and B. A. Joyce, Appl. Phys. **A33**, 87 (1984).
- 39 H. Jorke, Surf. Sci. **193**, 569 (1988).
- 40 M. Copel, C. Reuter, E. Kaxiras, and R. M. Tromp, Phys. Rev. Lett. **63**, 632 (1989).
- 41 N. Usami, S. Fukatsu, and Y. Shiraki, Appl. Phys. Lett. **63**, 388-390 (1993).
- 42 K. Sakamoto, K. Miki, T. Sakamoto, H. Yamaguchi, H. Oyanagi, H. Matsuhata, and K. Kyoya, Thin Solid Films **222**, 112 (1992).
- 43 G. Ohta, S. Fukatsu, Y. Ebuchi, T. Hattori, N. Usami, and Y. Shiraki, Appl. Phys. Lett. **65**, 2975 (1994).
- 44 K. Nakagawa, A. Nishida, Y. Kimura, and T. Shimada, J. Cryst. Growth **150**, 939 (1994).
- 45 A. Sakai, and T. Tatsumi, Appl. Phys. Lett. **64**, 52 (1994).
- 46 Y. Ebuchi, K. Amano, T. Hattori, S. Ohtake, N. Usami, and Y. Shiraki, *The 56th annual meeting of Japan Society of Applied Physics, Kanazawa (in Japanese)*

- 47 K. Terashima, M. Tajima, and T. Tatsumi, *Appl. Phys. Lett.* **57**, 1925 (1990).
- 48 J.-P. Noël, N.L. Rowell, D.C. Houghton, and D.D. Perovic, *Appl. Phys. Lett.* **57**, 1037 (1990).
- 49 J.-P. Noël, N.L. Rowell, D. C. Houghton, A. Wang, and D. D. Perovic, *Appl. Phys. Lett.* **61**, 690 (1992).
- 50 T.D. Steiner, R.L. Hengehold, Y.K. Yeo, D.J. Godbey, E. Thompson, and G.S. Pomrenke, *J. Vac. Sci. and Technol.* **B10**, 924 (1992).
- 51 J. Spitzer, K. Thonke, R. Sauer, H. Kibbel, H.-J. Herzog, and E. Kasper, *Appl. Phys. Lett.* **60**, 1729 (1992).
- 52 N. Usami, S. Fukatsu, and Y. Shiraki, *Appl. Phys. Lett.* **61**, 1706 (1992).
- 53 J. Brunner, U. Menczgar, M. Gail, E. Friess, and G. Abstreiter, *Thin Solid Films* **222**, 27 (1992).
- 54 J. C. Sturm, H. Manoharan, L. C. Lenchyshyn, M. L. Thewalt, N. L. Rowell, J.-P. Noël, and D. C. Houghton, *Phys. Rev. Lett.* **66**, 1362 (1991).
- 55 X. Xiao, C. W. Liu, J. C. Sturm, L. C. Lenchyshyn, M. L. W. Thewalt, R. B. Gregory, and P. Fejes, *Appl. Phys. Lett.*, **60**, 2135 (1992).
- 56 L. Vescan, A. Hartmann, K. Schmidt, Ch. Dieker, H. Luth, and W. Jäger, *Appl. Phys. Lett.* **60**, 2183 (1992).
- 57 S. Fukatsu, H. Yoshida, A. Fujiwara, Y. Takahashi, Y. Shiraki, and R. Ito, *Appl. Phys. Lett.* **61**, 804 (1992).
- 58 S. Fukatsu, N. Usami, K. Fujita, H. Yaguchi, Y. Shiraki, and R. Ito, *J. Cryst. Growth* **127**, 401-405 (1993).
- 59 H. Sunamura, S. Fukatsu, N. Usami, and Y. Shiraki, *Appl. Phys. Lett.* **63**, 1651-1653 (1993).
- 60 H. Sunamura, S. Fukatsu, N. Usami, and Y. Shiraki, *Jpn. J. Appl. Phys.* **33**, 2344-2347 (1994).
- 61 S. Fukatsu, and Y. Shiraki, *Appl. Phys. Lett.* **63**, 2378 (1993).
- 62 L. C. Lenchyshyn, M. L. Thewalt, D. C. Houghton, J. -P. Noël, N. L. Rowell, J. C. Sturm, and X. Xiao, *Phys. Rev.* **B47**, 4009 (1993).
- 63 S. Fukatsu, *Solid-State Electron.* **37**, 817 (1994).
- 64 S. Fukatsu, H. Sunamura, and Y. Shiraki, *J. Vac. Sci. Technol.* **B12**, 1160 (1994).
- 65 D. K. Nayak, N. Usami, H. Sunamura, S. Fukatsu, and Y. Shiraki, *Solid-State Electronics* **37**, 933 (1994).
- 66 F. Issiki, S. Fukatsu, and Y. Shiraki, *Appl. Phys. Lett.* **67**, 1048 (1995).
- 67 A. Zrenner, *Festkörperprobleme* **32**, 61 (1992).
- 68 A. Zrenner, L. V. Butov, M. Hagn, G. Abstreiter, G. Böhm, and G. Weimann, *Phys. Rev. Lett.* **72**, 3382 (1994).
- 69 E. A. Fitzgerald, Y. -H. Xie, M. L. Green, D. Brasen, A. R. Kortan, J. Michel, Y. -J. Mi, and B. E. Weir, *Appl. Phys. Lett.* **59**, 811 (1991).
- 70 R. Sauer, J. Weber, J. Stolz, *Appl. Phys.* **A36**, 1 (1985).
- 71 G. Bastard, "Wave mechanics applied to semiconductor heterostructures", Les Editions de Physique (1988).
- 72 J. Feldmann, G. Peter, E. O. Göbel, P. Dawson, K. Moore, C. Foxon, R. J. Elliott, *Phys. Rev. Lett.* **59**, 2337 (1987).
- 73 H. Akiyama, S. Koshiba, T. Someya, K. Wada, H. Noge, Y. Nakamura, T. Inoshita, A. Shimizu, and H. Sakaki, *Phys. Rev. Lett.* **72**, 924 (1994).
- 74 M. Grundmann, J. Christen, M. Joschko, O. Stier, D. Bimberg, and E. Kapon, *Semicon. Sci. Technol.* **9**, 1939 (1994).
- 75 M. Sugawara, *Phys. Rev.* **B51**, 10743 (1995).
- 76 P. Schittenhelm, M. Gail, J. Brunner, J. F. Nützel, and G. Abstreiter, *Appl. Phys. Lett.* **67**, 1292 (1995).
- 77 See example; H. Sakaki, *Surf. Sci.* **267**, 623 (1992).
- 78 E. Kapon, K. Kash, E. M. Clausen, Jr., D. M. Hwang, and E. Colas, *Appl. Phys. Lett.* **60**, 477 (1992).
- 79 S. Simhony, E. Kapon, E. Colas, D. M. Hwang, N. G. Stoffel, and P. Worland, *Appl. Phys. Lett.* **60**, 477 (1992).
- 80 J. Brunner, T. S. Rupp, H. Gossner, R. Ritter, I. Eisele, and G. Abstreiter, *Appl. Phys. Lett.* **64**, 994 (1994).
- 81 M. Tanaka, and H. Sakaki, *Appl. Phys. Lett.* **54**, 1326 (1989).
- 82 L. Pfeiffer, K. W. West, H. L. Stormer, J. P. Eisenstein, K. W. Baldwin, D. Gershoni, and J. Spector, *Appl. Phys. Lett.* **56**, 1697 (1990).
- 83 T. Fukui, S. Ando, and Y. K. Fukai, *Appl. Phys. Lett.* **57**, 1209 (1990).
- 84 S. Tsukamoto, Y. Nagamune, M. Nishioka, and Y. Arakawa, *Appl. Phys. Lett.* **62**, 49 (1993).
- 85 L. Vescan, C. Dieker, A. Hartmann, and A. van der Hart, *Semicond. Sci. Technol.* **9**, 387 (1994).
- 86 D. Leonard, M. Krishnamurthy, C. M. Reaves, S. P. Denbars, and P. M. Petroff, *Appl. Phys. Lett.* **63**, 3203 (1993).
- 87 R. Nötzel, N. N. Ledentsov, L. Däweritz, M. Hohenstein, and K. Ploog, *Phys. Rev. Lett.* **67**, 3812 (1991).
- 88 J. M. Gérard, in "Confined electrons and photons: new physics and applications" C. Weisbuch and E. Burnstein eds., NATO ASI series, Plenum (1994).
- 89 T. Mine, N. Usami, Y. Shiraki, and S. Fukatsu, *J. Cryst. Growth* **150**, 1033 (1995).
- 90 S. Fukatsu, H. Akiyama, Y. Shiraki, and H. Sakaki, *J. Cryst. Growth* **157**, 1 (1995).
- 91 H. Hillmer, A. Forchel, S. Hansman, M. Morohashi, E. Lopez, H. P. Meier, and K. Ploog, *Phys. Rev.* **B39**, 10901 (1989).
- 92 H. Hirayama, T. Tatsumi, and N. Aizaki, *Appl. Phys. Lett.* **52**, 2242 (1988).

- 93 H. Hirayama, M. Hiroi, K. Koyama, and T. Tatsumi, *Appl. Phys. Lett.* **56**, 1107 (1990).
- 94 Y. Arakawa, and H. Sakaki, *Appl. Phys. Lett.* **40**, 939 (1982).
- 95 J.-Y. Marzin, J.-M. Gérard, A. Izraël, D. Barrier, and G. Bastard, *Phys. Rev. Lett.* **73**, 716 (1994).
- 96 M. Grundmann, J. Christen, N. N. Lendenstov, J. Böhrer, D. Bimberg, S. S. Ruvimov, P. Werner, U. Richter, U. Gösele, J. Heydenreich, V. M. Ustinov, A. Yu. Egorov, A. E. Zhukov, P. S. Kop'ev, and Zh. I. Alferov, *Phys. Rev. Lett.* **74** 4043 (1995).
- 97 M. Notomi, T. Furuta, H. Kamada, J. Temmyo, and T. Tamamura, *Phys. Rev.* **B53**, 15743 (1996).
- 98 M. Nishioka, F. Sogawa, M. Kitamura, R. Schur, and Y. Arakawa, *Ext. Abs. of the 1996 Int. Conf. on SSDM*, 199 (1996).
- 99 G. Yusa, and H. Sakaki, *IEEE Electron. Lett.* **32**, 491 (1996).
- 100 K. Kash, J. M. Worlock, M. D. Sturge, P. Grabbe, J. P. Harbison, A. Scherer, and P. S. D. Lin, *Appl. Phys. Lett.* **53**, 782 (1988).
- 101 I.-H. Tan, R. Mirin, V. Jayaraman, S. Shi, E. Hu, and J. Bowers, *Appl. Phys. Lett.* **61**, 300 (1992).
- 102 H. Sunamura, Y. Shiraki, and S. Fukatsu, *J. Cryst. Growth* **150**, 1065 (1995).
- 103 Q. Xie, A. Madhukar, P. Chen, and N. P. Kobayashi, *Phys. Rev. Lett.* **75**, 2542 (1996).
- 104 J. Tersoff, C. Teichert, and M. G. Lagally, *Phys. Rev. Lett.* **76** 1675 (1995).

## List of Awards, Publications, and Presentations

### Awards

- (1) Young Researcher Award of 1993 International Conference on Solid State Devices and Materials, August 1993.
- (2) Engineering Foundation Conference Fellowship on Silicon Heterostructures: From Physics to Devices, September 1997.

### Author publications

#### Regular papers

- (1) N. Usami, S. Fukatsu, and Y. Shiraki, "Observation of deep-level-free band edge luminescence and quantum confinement in strained  $\text{Si}_{1-x}\text{Ge}_x/\text{Si}$  single quantum well structures grown by solid source molecular beam epitaxy", *Appl. Phys. Lett.* **61**, 1706-1709 (1992).
- (2) N. Usami, S. Fukatsu, and Y. Shiraki, "Abrupt compositional transition in luminescent  $\text{Si}_{1-x}\text{Ge}_x/\text{Si}$  quantum well structures fabricated by segregant assisted growth using Sb adlayer", *Appl. Phys. Lett.* **63**, 388-390 (1993).
- (3) N. Usami, T. Mine, S. Fukatsu, and Y. Shiraki, "Realization of crescent-shaped SiGe quantum wire structures on a V-groove patterned Si substrate by gas-source Si molecular beam epitaxy", *Appl. Phys. Lett.* **63**, 2789-2791 (1993).
- (4) N. Usami, T. Mine, S. Fukatsu, and Y. Shiraki, "Optical anisotropy in wire-geometry SiGe layers grown by gas-source selective epitaxial growth technique", *Appl. Phys. Lett.* **64**, 1126-1128 (1994).
- (5) N. Usami, T. Mine, S. Fukatsu, and Y. Shiraki, "Fabrication of SiGe/Si quantum wire structures on a V-groove patterned Si substrate by gas-source Si molecular beam epitaxy", *Solid-State Electron.* **37**, 539-541 (1994).
- (6) N. Usami, S. Fukatsu, and Y. Shiraki, "Photoluminescence of  $\text{Si}_{1-x}\text{Ge}_x/\text{Si}$  quantum wells with abrupt interfaces formed by segregant-assisted growth", *Jpn. J. Appl. Phys.* **33**, 2304-2306 (1994).
- (7) N. Usami, H. Sunamura, T. Mine, S. Fukatsu, and Y. Shiraki, "Strain-induced lateral band gap modulation in  $\text{Si}_{1-x}\text{Ge}_x/\text{Si}$  quantum well and quantum wire structures", *J. Cryst. Growth* **150**, 1065-1069 (1995).
- (8) N. Usami, H. Akiyama, Y. Shiraki, and S. Fukatsu, "Dynamics of exciton diffusion in SiGe quantum wells on a V-groove patterned Si substrate", *Phys. Rev.* **B52**, 5132-5135 (1995).
- (9) N. Usami, F. Issiki, D. K. Nayak, Y. Shiraki, and S. Fukatsu, "Enhancement of radiative recombination in Si-based quantum wells with neighboring confinement structure", *Appl. Phys. Lett.* **67**, 524-526 (1995).

- (10) N. Usami, Y. Shiraki, and S. Fukatsu, "Intense photoluminescence from Si-based quantum well structures with neighboring confinement structure", *J. Cryst. Growth* **157**, 27-30 (1995).
- (11) N. Usami, Y. Shiraki, S. Fukatsu, "Role of heterointerface on enhancement of no-phonon luminescence in Si-based neighboring confinement structure", *Appl. Phys. Lett.* **68**, 2340-2342 (1996).
- (12) N. Usami, H. Akiyama, Y. Shiraki, and S. Fukatsu, "Exciton diffusion dynamics in SiGe/Si quantum wells on a V-groove patterned Si substrate", *Solid-State Electron.* **40**, 733-736 (1996).
- (13) N. Usami, W. Pan, H. Yaguchi, R. Ito, K. Onabe, H. Akiyama, and Y. Shiraki, "Time-resolved photoluminescence study on AlGaAs spontaneous vertical quantum well structures", *Appl. Phys. Lett.* **68**, 3221-3223 (1996).
- (14) N. Usami, Y. Shiraki, and S. Fukatsu, "Spectroscopic study of Si-based quantum wells with neighboring confinement structure", *Semicon. Sci. Technol.* **12**, 1596 (1997).
- (15) N. Usami, W. Pan, H. Yaguchi, K. Onabe, and Y. Shiraki, "Exciton diffusion dynamics in quantum nanostructures on V-groove patterned substrates", *Superlattice and Microstructures* (to be published in vol. **24** in 1998).
- (16) N. Usami, T. Sugita, T. Ohta, H. Ito, K. Uchida, Y. Shiraki, F. Minami, and N. Miura, "In-plane potential modulation in tensilely strained AlGaP-based neighboring confinement structure", *Physica B* (to be published in 1998).
- (17) N. Usami, J. Arai, E. S. Kim, K. Ota, T. Hattori, and Y. Shiraki, "Control of island formation using overgrowth techniques on cleaved edges of strained multiple quantum wells and selective epitaxy on patterned substrates", *Physica B* (to be published in 1998).
- (18) N. Usami, M. Miura, H. Sunamura, and Y. Shiraki, "Photoluminescence from pure-Ge/pure-Si neighboring confinement structure", *J. Vac. Sci. and Technol.* (submitted).

#### Proceedings

- (1) N. Usami, S. Fukatsu, and Y. Shiraki, "Solid source molecular beam epitaxial growth of highly luminescent Si<sub>1-x</sub>Ge<sub>x</sub>/Si quantum well structures", *Ext. Abs. of the 1992 Int. Conf. on Solid State Devices and Material*, 677-679 (1992).
- (2) N. Usami, T. Mine, S. Fukatsu, and Y. Shiraki, "Gas-source molecular beam epitaxial growth of crescent-shaped SiGe quantum wire arrays on a V-groove patterned Si substrate", *Ext. Abs. of the 1993 Int. Conf. on Solid State Devices and Material*, 228-230 (1993).
- (3) N. Usami, S. Fukatsu, and Y. Shiraki, "Formation of luminescent Si<sub>1-x</sub>Ge<sub>x</sub>/Si quantum wells with abrupt interfaces by segregant-assisted growth", *Ext. Abs. of the 1993 Int. Conf. on Solid State Devices and Material*, 243-245 (1993).
- (4) N. Usami, T. Ohta, F. Issiki, Y. Shiraki, and S. Fukatsu, "Enhancement of no-phonon luminescence from indirect semiconductors with neighboring confinement structure", *23rd Int. Conf. on The Phys. of Semicon.* **3**, 1843-1846 (1996).

#### Co-author publications

##### Regular papers

- (1) S. Fukatsu, N. Usami, H. Yoshida, A. Fujiwara, Y. Takahashi, Y. Shiraki, and R. Ito, "Band edge luminescence in SiGe/Si single quantum wells grown on Si(111) substrates by solid-source molecular beam epitaxy", *Jpn. J. Appl. Phys.* **31**, 1015-1017 (1992).
- (2) S. Fukatsu, N. Usami, T. Chinzei, Y. Shiraki, A. Nishida, and K. Nakagawa, "Electroluminescence in strained SiGe/Si quantum well structures grown by solid-source Si molecular beam epitaxy", *Jpn. J. Appl. Phys.* **31**, 1018-1020 (1992).
- (3) S. Fukatsu, N. Usami, H. Yoshida, A. Fujiwara, Y. Takahashi, Y. Shiraki, and R. Ito, "Quantum size effect of excitonic band-edge luminescence in strained SiGe/Si single quantum well structures grown by gas-source molecular beam epitaxy", *Jpn. J. Appl. Phys.* **31**, 1319-1321 (1992).
- (4) S. Fukatsu, N. Usami, and Y. Shiraki, "Photogeneration and transport of carriers in strained SiGe/Si quantum well structures", *Jpn. J. Appl. Phys.* **31**, L1525-L5281 (1992).
- (5) D. K. Nayak, N. Usami, H. Sunamura, S. Fukatsu, and Y. Shiraki, "Band-edge photoluminescence of SiGe/strained-Si/SiGe type-II quantum wells on Si(100)", *Jpn. J. Appl. Phys.* **32**, L1391-1393 (1992).
- (6) S. Fukatsu, H. Yoshida, N. Usami, A. Fujiwara, Y. Takahashi, Y. Shiraki, and R. Ito, "Systematic blue shift of exciton luminescence in strained SiGe/Si quantum well structures grown by gas source molecular beam epitaxy", *Thin Solid Films* **222**, 1-4 (1992).
- (7) K. Fujita, S. Fukatsu, N. Usami, Y. Shiraki, H. Yaguchi, R. Ito, and K. Nakagawa, "Self-modulating Sb incorporation in Si/SiGe superlattices during molecular beam epitaxial growth", *Surf. Sci.* **295**, 335-339 (1993).
- (8) S. Fukatsu, N. Usami, K. Fujita, H. Yaguchi, Y. Shiraki, and R. Ito, "Is low temperature growth the solution to abrupt interface formation?", *J. Cryst. Growth* **127**, 401-405 (1993).
- (9) S. Fukatsu, N. Usami, H. Yoshida, A. Fujiwara, Y. Takahashi, Y. Shiraki, and R. Ito, "Intense photoluminescence from strained SiGe/Si quantum well structures", *J. Cryst. Growth* **127**, 489-493 (1993).
- (10) S. Fukatsu, N. Usami, Y. Shiraki, A. Nishida, and K. Nakagawa, "Observation of electroluminescence above room temperature in strained p-type SiGe/Si(111) multiple quantum wells", *J. Cryst. Growth* **127**, 1083-1087 (1993).
- (11) S. Fukatsu, N. Usami, and Y. Shiraki, "Luminescence from strained SiGe/Si quantum wells grown by Si molecular beam epitaxy", *Jpn. J. Appl. Phys.* **32**, 1502-1507 (1993).
- (12) S. Fukatsu, N. Usami, and Y. Shiraki, "Luminescence from SiGe/Si quantum wells grown by Si molecular beam epitaxy", *J. Vac. Sci. and Technol.* **B11**, 895-898 (1993).
- (13) S. Fukatsu, N. Usami, Y. Shiraki, A. Nishida, and K. Nakagawa, "High temperature operation of strained p-type SiGe/Si(111) multiple-quantum-well light emitting diode grown by solid-source Si molecular beam epitaxy", *Appl. Phys. Lett.* **63**, 967-969 (1993).

- (14) Y. Yamashita, K. Maeda, K. Fujita, N. Usami, K. Suzuki, S. Fukatsu, Y. Mera, and Y. Shiraki, "Dislocation glide motion in heteroepitaxial thin films of SiGe/Si(100)", *Phys. Mag. Lett.* **67**, 165-171 (1993).
- (15) H. Sunamura, S. Fukatsu, N. Usami, and Y. Shiraki, "Luminescence study on interdiffusion in strained SiGe/Si quantum wells grown by gas-source molecular beam epitaxy", *Appl. Phys. Lett.* **63**, 1651-1653 (1993).
- (16) Y. Kato, S. Fukatsu, N. Usami, and Y. Shiraki, "Hybrid Si molecular beam epitaxial regrowth for a strained Si<sub>1-x</sub>Ge<sub>x</sub>/Si single-quantum-well electroluminescence device", *Appl. Phys. Lett.* **63**, 2414-2416 (1993).
- (17) D. K. Nayak, N. Usami, S. Fukatsu, and Y. Shiraki, "Band-edge photoluminescence of SiGe/strained-Si/SiGe type-II quantum wells on Si(100)", *Appl. Phys. Lett.* **63**, 3509-3511 (1993).
- (18) D. K. Nayak, N. Usami, H. Sunamura, S. Fukatsu, and Y. Shiraki, "Band-edge photoluminescence of SiGe/strained-Si/SiGe type-II quantum wells on Si(100)", *Solid-state Electron.* **37**, 933-936 (1994).
- (19) D. K. Nayak, N. Usami, S. Fukatsu, and Y. Shiraki, "Photoluminescence of Si/SiGe/Si quantum wells on separation by oxygen implantation substrate", *Appl. Phys. Lett.* **64**, 2373-2375 (1994).
- (20) S. Fukatsu, N. Usami, Y. Kato, H. Sunamura, Y. Shiraki, H. Oku, T. Ohnishi, Y. Ohmori, and K. Okumura, "Gas-source MBE and luminescence characterization of strained SiGe/Si quantum wells", *J. Cryst. Growth* **136**, 315-321 (1994).
- (21) Y. Kato, S. Fukatsu, N. Usami, and Y. Shiraki, "A SiGe/Si single quantum well p-i-n structure grown by solid and gas source hybrid Si molecular beam epitaxy", *J. Cryst. Growth* **136**, 355-360 (1994).
- (22) H. Sunamura, S. Fukatsu, N. Usami, and Y. Shiraki, "Optical detection of interdiffusion in strained Si<sub>1-x</sub>Ge<sub>x</sub>/Si quantum well structures", *Jpn. J. Appl. Phys.* **33**, 2344-2347 (1994).
- (23) G. Ohta, S. Fukatsu, Y. Ebuchi, T. Hattori, N. Usami, and Y. Shiraki, "Abrupt Si/Ge interface formation using atomic hydrogen in Si molecular beam epitaxy", *Appl. Phys. Lett.* **65**, 2975-2977 (1994).
- (24) H. Sunamura, N. Usami, Y. Shiraki, and S. Fukatsu, "Island formation during growth of Ge on Si(100): A study using photoluminescence spectroscopy", *Appl. Phys. Lett.* **66**, 3024-3026 (1995).
- (25) T. Mine, N. Usami, Y. Shiraki, and S. Fukatsu, "Crucial role of Si buffer layer quality in the photoluminescence efficiency of strained Si<sub>1-x</sub>Ge<sub>x</sub>/Si quantum wells", *J. Cryst. Growth* **150**, 1033-1037 (1995).
- (26) V. Higgs, E. C. Lightowers, N. Usami, Y. Shiraki, T. Mine, and S. Fukatsu, "Cathodoluminescence investigation of SiGe quantum wires fabricated on V-groove patterned Si substrates", *J. Cryst. Growth* **150**, 1070-1073 (1995).

- (27) G. Ohta, S. Fukatsu, N. Usami, Y. Shiraki, and T. Hattori, "Anomalous spectral shift of photoluminescence from MBE-grown strained SiGe/Si quantum wells mediated by atomic hydrogen", *J. Cryst. Growth* **157**, 36-39 (1995).
- (28) J. Y. Kim, S. Fukatsu, N. Usami, Y. Shiraki, "Field-driven blue shift of excitonic photoluminescence in Si-Ge quantum wells and superlattices", *J. Cryst. Growth* **157**, 40-44 (1995).
- (29) H. Sunamura, S. Fukatsu, N. Usami, Y. Shiraki, "Photoluminescence investigation on growth mode changeover of Ge on (100)", *J. Cryst. Growth* **157**, 265-269 (1995).
- (30) V. Higgs, E. C. Lightowers, N. Usami, Y. Shiraki, T. Mine, and S. Fukatsu, "Characterization of SiGe quantum wires by cathodoluminescence imaging and spectroscopy", *Appl. Phys. Lett.* **67**, 1709-1711 (1995).
- (31) W. Pan, H. Yaguchi, K. Onabe, R. Ito, N. Usami, and Y. Shiraki, "Rectangular AlGaAs/AlAs quantum wires using spontaneous vertical quantum-wells", *Jpn. J. Appl. Phys.* **35**, 1214-1216 (1996).
- (32) H. Sunamura, N. Usami, Y. Shiraki, and S. Fukatsu, "Observation of lateral confinement effect in Ge quantum wires self-aligned at step edges on Si(100)", *Appl. Phys. Lett.* **68**, 1847-1849 (1996).
- (33) S. Fukatsu, N. Usami, and Y. Shiraki, "Improved luminescence quality with an asymmetric confinement potential in Si-based type-II quantum wells grown on a graded SiGe relaxed buffer", *J. Vac. Sci. Technol.* **B14**, 2387-2390 (1996).
- (34) Y. Shiraki, H. Sunamura, N. Usami, and S. Fukatsu, "Formation and optical properties of SiGe/Si quantum structures", *Appl. Surf. Sci.* **102**, 263-271 (1996).
- (35) N. Sekine, K. Hirakawa, F. Sogawa, Y. Arakawa, N. Usami, Y. Shiraki, and T. Katoda, "Ultrashort lifetime photocarriers in Ge thin films", *Appl. Phys. Lett.* **68**, 3419-3421 (1996).
- (36) L. K. Bera, S. K. Ray, D. K. Nayak, N. Usami, Y. Shiraki, and C. K. Maiti, "Electrical properties of oxides grown on strained Si using microwave N<sub>2</sub>O plasma", *Appl. Phys. Lett.* **70**, 66-68 (1997).
- (37) L. K. Bera, M. Mukhopadhyay, S. K. Ray, D. K. Nayak, N. Usami, Y. Shiraki, and C. K. Maiti, "Oxidation of strained Si in a microwave electron cyclotron resonance plasma", *Appl. Phys. Lett.* **70**, 217-219 (1997).
- (38) E. S. Kim, N. Usami, and Y. Shiraki, "Anomalous luminescence peak shift of SiGe/Si quantum well induced by self-assembled Ge islands", *Appl. Phys. Lett.* **70**, 295-297 (1997).
- (39) E. S. Kim, N. Usami, H. Sunamura, Y. Shiraki, and S. Fukatsu, "Luminescence study on Ge islands a stressors on SiGe/Si quantum well", *J. Cryst. Growth* **175/176**, 519 (1997).
- (40) H. Sunamura, S. Fukatsu, N. Usami, and Y. Shiraki, "Anomalous photoluminescence of pure-Ge/Si type-II coupled quantum wells", *Thin Solid Films* **294**, 336 (1997).
- (41) P. Reimer, J. H. Li, Y. Yamaguchi, O. Sakata, H. Hashizume, N. Usami, and Y. Shiraki, "Interfacial roughness of SiGe/Si multilayer structures on Si(111) probed by x-ray scattering", *J. Phys. Cond. Matt.* **9**, 4521 (1997).

- (42) D. K. Nayak, N. Usami, S. Fukatsu, and Y. Shiraki, "Study of the optical properties of SOI substrate" *J. Appl. Phys.* **81**, 3484 (1997).
- (43) T. Ohta, N. Usami, F. Issiki, and Y. Shiraki, "Effects of tensile strain on optical properties of AlGaP-based neighboring confinement structure" *Semicon. Sci. and Technol.* **12**, 881 (1997).
- (44) J. Arai, N. Usami, K. Ota, Y. Shiraki, A. Ohga, and T. Hattori, "Precise control of the island formation using overgrowth technique on cleaved-edge of strained multiple quantum wells", *Appl. Phys. Lett.* **70**, 2981 (1997).
- (45) J. Arai, A. Ohga, T. Hattori, N. Usami, and Y. Shiraki, "Optical investigation of growth mode of Ge thin films on Si(110) substrates" *Appl. Phys. Lett.* **71**, 785 (1997).
- (46) T. Ohta, N. Usami, F. Issiki, and Y. Shiraki, "Effects of tensile strain on optical properties of AlGaP-based neighboring confinement structure", *Superlattice and Microstructures* (to be published in vol. **23** in 1998).
- (47) E. S. Kim, N. Usami, and Y. Shiraki, "Control of Ge dots in dimension and position by selective epitaxial growth and their optical properties", *Appl. Phys. Lett.* (to be published).
- (48) T. Sugita, N. Usami, and Y. Shiraki, "Enhanced no-phonon transition in indirect GaAsP/GaP quantum wells by insertion of monolayer AlP for electron localization", *J. Cryst. Growth* (to be published).
- (49) K. Ota, N. Usami, and Y. Shiraki, "Temperature dependence of microscopic photoluminescence spectra of quantum dots and quantum wells", *Physica B* (to be published).
- (50) H. Sunamura, N. Usami, Y. Shiraki, and S. Fukatsu, "A new strain-relieving microstructure in pure-Ge/Si short period superlattices", *J. Vac. Sci. Technol.* (submitted).

#### Proceedings

- (1) D. K. Nayak, N. Usami, S. Fukatsu, and Y. Shiraki, "Photoluminescence of SiGe quantum wells grown on SIMOX by gas source MBE", *Ext. Abs. of the 1994 Int. Conf. on Solid State Devices and Materials*, 745-747 (1994).
- (2) Y. Shiraki, S. Fukatsu, K. Fujita, and N. Usami, "Segregant-assisted growth of SiGe/Si heterostructures and their optical properties", *Mat. Res. Soc. Symp. Proc.* **318**, 191-200 (1994).
- (3) W. Pan, H. Yaguchi, K. Onabe, R. Ito, N. Usami, and Y. Shiraki, "The in situ growth of lateral confinement enhanced rectangular AlGaAs/AlAs quantum wires by utilizing the spontaneous vertical quantum wells", *Ext. Abs. of the 1995 Int. Conf. on Solid State Devices and Materials*, 737-739 (1995).
- (4) W. Pan, H. Yaguchi, K. Onabe, R. Ito, N. Usami, and Y. Shiraki, "Polarization properties of GaAsP/AlGaAs tensilely strained quantum wire structures grown on V-grooved GaAs substrate", *Inst. Phys. Conf. Ser.* **145**, 925-930 (1995).

- (5) Y. Shiraki, N. Usami, T. Mine, H. Akiyama, and S. Fukatsu, "Formation and properties of SiGe/Si quantum wire structures", *Low dimensional Structures prepared by Epitaxial Growth or regrowth on Patterned substrates*, edited by K. Eberl et al., 151-160 (1995).
- (6) E. S. Kim, N. Usami, and Y. Shiraki, "Strain effects of Ge islands on SiGe/Si quantum well", *Ext. Abs. of the 1996 Int. Conf. on Solid State Devices and Materials*, 425-427 (1996).
- (7) S. Fukatsu, N. Usami, H. Sunamura, Y. Shiraki, and R. Ito, "Physics and control of Si/Ge heterointerfaces" *Mat. Res. Soc. Proc.* **448**, 125 (1997).

#### Presentations at International Conferences

- (1) N. Usami, S. Fukatsu, and Y. Shiraki, "Solid source molecular beam epitaxial growth of highly luminescent Si<sub>1-x</sub>Ge<sub>x</sub>/Si quantum well structures", *1992 International Conference on Solid State Devices and Materials*, Aug. 1992, Tsukuba, Japan
- (2) N. Usami, T. Mine, S. Fukatsu, and Y. Shiraki, "Fabrication of SiGe/Si quantum wire structures on a V-groove patterned Si substrate by gas-source Si molecular beam epitaxy" *The Sixth International Conference on Modulated Semiconductor Structure*, Aug. 1993, Garmisch-Partenkirchen, Germany
- (3) N. Usami, T. Mine, S. Fukatsu, and Y. Shiraki, "Gas-source molecular beam epitaxial growth of crescent-shaped SiGe quantum wire arrays on a V-groove patterned Si substrate", *1993 International Conference on Solid State Devices and Materials*, Aug. 1993, Makuhari, Japan
- (4) N. Usami, S. Fukatsu, and Y. Shiraki, "Formation of luminescent Si<sub>1-x</sub>Ge<sub>x</sub>/Si quantum wells with abrupt interfaces by segregant-assisted growth", *1993 International Conference on Solid State Devices and Materials*, Aug. 1993, Makuhari, Japan
- (5) N. Usami, H. Sunamura, T. Mine, S. Fukatsu, and Y. Shiraki, "Strain-induced lateral band gap modulation in Si<sub>1-x</sub>Ge<sub>x</sub>/Si quantum well and quantum wire structures", *The Eighth International Conference on Molecular Beam Epitaxy*, 29 Aug. -2 Sept. 1994, Suita, Japan
- (6) N. Usami, F. Issiki, S. Fukatsu, and Y. Shiraki, "Intense photoluminescence from Si-based quantum well structures with neighboring confinement structure", *The Sixth International Conference on Silicon Molecular Beam Epitaxy*, 23-25 May 1995, Sirasbourg, France
- (7) N. Usami, H. Akiyama, T. Mine, Y. Shiraki, and S. Fukatsu, "Exciton diffusion in SiGe/Si quantum wells on a V-groove patterned Si substrate", *The Seventh International Conference on Modulated Semiconductor Structures*, 10-14 July 1995, Madrid, Spain
- (8) N. Usami, and Y. Shiraki, "Exciton diffusion dynamics in quantum nanostructures on V-groove patterned substrates" *Symp. of UK-Japan Int. Collaborative Research Project on Mesoscopic Electronics*, Mar. 1996, Kanakura, Japan

- (9) N. Usami, W. Pan, H. Yaguchi, K. Onabe, and Y. Shiraki  
"Exciton diffusion dynamics in quantum nanostructures on V-groove patterned substrates"  
*The Ninth Int. Conf. on Superlattice and Microstructures, 14-19 July 1996, Liège, Belgium*
- (10) N. Usami, T. Ohta, F. Issiki, Y. Shiraki, and S. Fukatsu  
"Enhancement of no-phonon luminescence from indirect semiconductors with neighboring confinement structure"  
*The 23rd International Conference on the Physics of Semiconductors., 21-26 July 1996, Berlin, Germany*
- (11) N. Usami, J. Arai, A. Ohga, H. Yaguchi, T. Hattori, and Y. Shiraki.  
"Photoluminescence from Ge thin films on Si(110) grown by solid-source molecular beam epitaxy".  
*The Seventh International Conference on Silicon Molecular Beam Epitaxy, 13-17 July 1997, Banff, Canada*
- (12) N. Usami, T. Sugita, T. Ohta, H. Ito, K. Uchida, Y. Shiraki, F. Minami, and N. Miura,  
"In-plane potential modulation in tensilely-strained AlGaP-based neighboring confinement structure".  
*The Eighth International Conference on Modulated Semiconductor Structures, 14-18 July 1997, Santa Barbara, USA*
- (13) N. Usami, J. Arai, E. S. Kim, K. Ota, T. Hattori, and Y. Shiraki,  
"Control of island formation using overgrowth technique on cleaved edges of strained multiple quantum wells and selective epitaxy on patterned substrates".  
*The Eighth International Conference on Modulated Semiconductor Structures, 14-18 July 1997, Santa Barbara, USA*
- (14) N. Usami, J. Arai, E. S. Kim, K. Ota, T. Hattori, and Y. Shiraki.  
"Control of island formation using overgrowth technique on cleaved edges of strained multiple quantum wells and selective epitaxy on patterned substrates".  
*The Eighth International Conference on Modulated Semiconductor Structures, 14-18 July 1997, Santa Barbara, USA*
- (15) N. Usami, M. Miura, H. Sunamura, and Y. Shiraki,  
"Photoluminescence from pure-Ge/pure-Si neighboring confinement structure",  
*The Second International Symposium on Silicon Heterostructures: From Physics to Devices, 15-19 September 1997, Castelvecchio Pascoli, Italy*

分子生物学